NONHYDROSTATIC ADIABATIC KERNEL FOR HIRLAM
Part II
Anelastic, hybrid–coordinate, explicit–Eulerian model

Aarne Männik
Tartu University, Estonia
aarne@aai.ee

Rein Rõõm
Tartu Observatory, Estonia
room@aai.ee

Introduction

Part II continues the description of the numerical model of atmospheric dynamics, designed as the nonhydrostatic extension to the hydrostatic kernel of HIRLAM. The theoretical concept, initiated in Part I, will be brought to numerical codes. The anelastic hybrid–coordinate model is formulated both in the continuous and discrete representations, and the numerical code with the explicit–Eulerian time stepping scheme is implemented in the HIRLAM environment. The paper ends with numerical examples, demonstrating the capabilities of the model.

The numerical code is based on the former results, obtained by Xue and Thorpe (1991), Miranda and James (1992), and, with respect to pressure adjustment, Rõõm (1997). However, there are several modifications in comparison with those papers. Instead of the sigma coordinates, the present model makes use of the more general hybrid coordinates of HIRLAM. Also, the whole vertical extent of the atmosphere is incorporated, and there is no artificial upper boundary in the present approach. However, the most

fundamental difference is in the level and mode of simplifications. In the above-cited papers the Miller-Pearce variant (Miller and Pearce, 1974) is applied, which makes use of the background separation and linearization of the energy conversion term. We make use of the more general White model (White, 1989) without linearization in that term. At the same time, some linearization is introduced at surface pressure handling, which is needed for surface pressure adjustment.

In the development of numerical code, the main attention is paid to the creation of the elliptic solver for the baric geopotential equation. It is different from the hydrostatic semi-implicit scheme which makes use of the Helmholtz equation. In this case we have to deal with the Poisson equation. The main difference is that the Poisson equation does not have any large diagonal part like the Helmholtz equation does, and, as a result, the iterative scheme of the latter is not applicable here. The present solution algorithm is based on the scheme, initiated by Xue and Thorpe (1991), and further elaborated for three-dimensional domain by Miranda and James (1992). The essential quality of that scheme is the application of fast discrete Fourier transformation in horizontal with consequent numerical inversion of one-dimensional Laplacians for each Fourier mode in vertical. The lateral boundary–condition treatment in their approach follows Williams (1969). In this approach we have gone one step further, and apply an orthogonal basis in all three coordinates, including the vertical hybrid coordinate. The nonhomogeneous boundary conditions are handled by introduction of singular sources on lateral and bottom boundaries. Due to such a modification, the developed inversion algorithm becomes a rather universal tool for solution of Poisson equations in horizontally rectangular domains with general boundary conditions. At the same time, the scheme is not more time consuming than the original Xue-Thorpe approach.

The hybrid-coordinate representation of the nonhydrostatic model follows the notation of the hydrostatic HIRLAM, presented in the Manual (Källén 1996). A few exceptions are:

(i) instead of $\vec{v}_h$, the notation $\mathbf{v}$ will be used for the horizontal wind velocity.

(ii) instead of $R_d T_v$, notation RT (with the "moist" R and true T) will be used; $\varkappa = R/c_p$ corresponds to moist air.

(iii) Special notation $m \equiv \partial p/\partial \eta$ is used.

(iv) Energy conservation, disregarded by the hydrostatic scheme in some minor terms of adiabatic dynamics, is restored following Haltiner and Williams (1980).

The section and formula numbering is continued from Part I. The first section in this part has number 4; "(3.4.1)" represents reference to the formula (3.4.1) in section 3 of Part I, etc.

4 Continuous anelastic hybrid-coordinate model

4.1 Diagnostics

The vertical η-coordinate $0 < \eta < 1$ is defined via mapping $\eta \to p$:

$$p = A(\eta) + B(\eta)\overline{p}_0 \ . \tag{4.1.1}$$

where $\overline{p}_0(\mathbf{x}, t)$ is a given (fixed or externally driven) background surface pressure field, and $A(\eta) \geq 0$, $B(\eta) \geq 0$ are the appropriate weights, which satisfy boundary conditions

$$A(0) = A(1) = 0 \ , \qquad B(0) = 0 \ , \quad B(1) = 1 \ . \tag{4.1.2}$$

Thus, the vertical domain in the pressure coordinates is (3.4.1), and $\eta = 1$ corresponds to $p = \overline{p}_0$.

The horizontal domain is a part of the globe with spherical coordinates $\{\lambda,\ \theta\}$

$$-\Lambda < \lambda < \Lambda \ , \qquad -\Theta < \theta < \Theta \ . \tag{4.1.3}$$

However, the horizontal coordinates, used at the definition of gradient operators, are $x = a\lambda$ and $y = a\theta$, with a as the mean radius of the Earth. the physical differences along the parallel and meridian are

$$dX = a\cos\theta d\lambda = h_x dx \quad dY = ad\theta = h_y dy \ , \tag{4.1.4}$$

where

$$h_x = \cos\theta \ , \quad h_y = 1$$

are the metrical coefficients. Thus, the curvilinear hybrid coordinates are $\{x\ , y\ , \eta\ \}$, whereas the velocity components are $u = h_x dx/dt$, $v = h_y dy/dt$, $\dot{\eta} = d\eta/dt$.

The hybrid-coordinate density m is related to the pressure-coordinate density n via $md\eta = ndp$, and for the anelastic model with $n = 1$

$$m = \frac{\partial p}{\partial \eta} \ . \tag{4.1.5}$$

In accordance with the definition (4.1.1), m depends on time (via $\overline{p}_0$), and the continuity equation for it is

$$\frac{\partial m}{\partial t} + \nabla \cdot (m\mathbf{v}) + \frac{\partial \dot{\eta} m}{\partial \eta} = 0 \ , \tag{4.1.6}$$

where the η-coordinate "horizontal" divergence of vector $\mathbf{a} = \{a_x, \ a_y\}$ is

$$\nabla \cdot \mathbf{a} = \frac{1}{h_x h_y} \left(\frac{\partial h_y a_x}{\partial x} + \frac{\partial h_x a_y}{\partial y} \right) \ . \tag{4.1.7}$$

From the definition (4.1.1)

$$\omega = m\dot{\eta} + B(\eta) \left(\frac{\partial \overline{p}_0}{\partial t} + \mathbf{v} \cdot \nabla \overline{p}_0 \right) \ , \tag{4.1.8}$$

or alternatively

$$\omega = m\dot{\eta} + \mathbf{v} \cdot \nabla p + \frac{\partial p}{\partial t} \ . \tag{4.1.8$'$}$$

Condition (2.4.3) and (3.4.2') give with the help of (4.1.8) boundary conditions for $\dot{\eta}$:

$$\dot{\eta} = 0 \qquad \text{at} \qquad \eta = 0 \qquad \text{and} \qquad \eta = 1 \ . \tag{4.1.9}$$

As a consequence, integration of (4.1.6) in vertical gives

$$\frac{\partial \overline{p_0}}{\partial t} + \int_0^1 \nabla \cdot (m\mathbf{v}) d\eta \ = 0 \ , \tag{4.1.10}$$

whereas integration of (4.1.6) in the the domain $[\eta, 1]$ yields

$$m\dot{\eta} = (1 - B) \frac{\partial \overline{p}_0}{\partial t} + \int_\eta^1 \nabla \cdot (m\mathbf{v}) d\eta \ . \tag{4.1.11}$$

Using (4.1.8'), the continuity equation (4.1.6) can be presented in the form

$$\hat{\mathbf{G}}^+ \cdot \mathbf{v} + \frac{1}{m} \frac{\partial \omega}{\partial \eta} = 0 \ , \tag{4.1.12}$$

where $\hat{\mathbf{G}}^+$ is the η-coordinate presentation of the pressure-coordinate "horizontal" divergence

$$\hat{\mathbf{G}}^+ \cdot \mathbf{v} \equiv \nabla_p \cdot \mathbf{v} = \frac{1}{m}\nabla \cdot (m\mathbf{v}) - \frac{1}{m}\frac{\partial(\mathbf{v} \cdot \nabla p)}{\partial \eta} \ , \tag{4.1.13}$$

which can be simplified to

$$\hat{\mathbf{G}}^+ \cdot \mathbf{v} = \nabla \cdot \mathbf{v} - \frac{1}{m}\frac{\partial \mathbf{v}}{\partial \eta} \cdot \nabla p \ , \tag{4.1.13$'$}$$

where the "horizontal" hybrid–coordinate gradient is

$$\nabla = \mathbf{i}^{\mathbf{x}}\frac{1}{h_x}\frac{\partial}{\partial x} + \mathbf{i}^{\mathbf{y}}\frac{1}{h_y}\frac{\partial}{\partial y} \ . \tag{4.1.14}$$

Thus, (4.1.12) is the hybrid-coordinate presentation of the anelastic condition (3.2.5).

The "horizontal" pressure-coordinate gradient is presented as

$$\hat{\mathbf{G}}\varphi \equiv \nabla_p \varphi = \nabla\varphi - \frac{1}{m}\frac{\partial \varphi}{\partial \eta}\nabla p \ . \tag{4.1.15}$$

The operators $\hat{\mathbf{G}}$ and $\hat{\mathbf{G}}^+$ are skew symmetric conjugates of each other:

$$\int_V dV m\varphi \hat{\mathbf{G}}^+ \cdot \mathbf{a} = -\int_V dV m\mathbf{a} \cdot \hat{\mathbf{G}}\varphi \tag{4.1.16}$$

for optional finite $\mathbf{a}$ and φ, where $dV = h_x h_y dx dy d\eta$, and V is the domain of integration. This relationship is useful in the discrete case for establishment of proper symmetry of the operators $\hat{\mathbf{G}}$ and $\hat{\mathbf{G}}^+$.

4.2 Dynamics

In the Eulerian presentation the equations of motion (3.2.3) – (3.2.4) are, after separation of momentum advection terms into the gradient, solenoidal and vertical parts,

$$\frac{\partial u}{\partial t} = F_u - \widehat{G}_x \phi \ , \tag{4.2.1}$$

$$\frac{\partial v}{\partial t} = F_v - \widehat{G}_y \phi \ , \tag{4.2.2}$$

$$\frac{\partial T}{\partial t} = F_T \ , \tag{4.2.3}$$

where $\widehat{G}_x$ and $\widehat{G}_y$ are the components of $\hat{\mathbf{G}}$:

$$\widehat{G}_x \phi \equiv \frac{1}{h_x} \left(\frac{\partial \phi}{\partial x} \right)_p = \frac{1}{h_x} \left(\frac{\partial \phi}{\partial x} - \frac{1}{m} \frac{\partial p}{\partial x} \frac{\partial \phi}{\partial \eta} \right)_\eta , \tag{4.2.4a}$$

$$\widehat{G}_y \phi \equiv \frac{1}{h_y} \left(\frac{\partial \phi}{\partial y} \right)_p = \frac{1}{h_y} \left(\frac{\partial \phi}{\partial y} - \frac{1}{m} \frac{\partial p}{\partial y} \frac{\partial \phi}{\partial \eta} \right)_\eta . \tag{4.2.4b}$$

F_u, F_v and F_T are the hydrostatic tendencies, which are those of the hydrostatic HIRLAM (with an exception that φ is the thermic geopotential rather than the hydrostatic one):

$$F_u = (f + \xi)\, v - \dot{\eta} \frac{\partial u}{\partial \eta} - \frac{1}{h_x} \left[RT \frac{\partial \ln p}{\partial x} + \frac{\partial}{\partial x} (\varphi + E) \right] + P_u + K_u, \tag{4.2.5}$$

$$F_v = (f + \xi)\, u - \dot{\eta} \frac{\partial v}{\partial \eta} - \frac{1}{h_y} \left[RT \frac{\partial \ln p}{\partial y} + \frac{\partial}{\partial y} (\varphi + E) \right] + P_v + K_v, \tag{4.2.6}$$

$$F_T = -\frac{u}{h_x} \frac{\partial T}{\partial x} - \frac{v}{h_y} \frac{\partial T}{\partial y} - \dot{\eta} \frac{\partial T}{\partial \eta} + \frac{\varkappa T \omega}{p} + P_T + K_T \ . \tag{4.2.7}$$

The vorticity and energy terms are here

$$\xi = \frac{1}{h_x h_y} \left(\frac{\partial h_y v}{\partial x} - \frac{\partial h_x u}{\partial y} \right) \tag{4.2.8}$$

$$E = \frac{1}{2} (u^2 + v^2) \ , \tag{4.2.9}$$

and P_x, K_x represent the tendencies from physical parametrization and horizontal diffusion (the sum $P_x + K_x$ corresponds to A_x in (3.1.6) - (3.1.7)).
The thermic geopotential (3.4.4b) is in the hybrid coordinates

$$\varphi = gh + \int_\eta^1 RT\frac{md\eta'}{p} \ . \tag{4.2.10}$$

The vertical momentum equation (3.2.2), which is required for the deduction of the ϕ-equation, is in hybrid coordinates (and in the Eulerian presentation)

$$\frac{\partial\omega}{\partial t} = F_\omega - \frac{p^2}{mH^2}\frac{\partial\phi}{\partial\eta} \tag{4.2.11}$$

where

$$F_\omega = A_\omega - \mathbf{v}\cdot\nabla\omega - \dot\eta\frac{\partial\omega}{\partial\eta} \ . \tag{4.2.12}$$

Differentiation of the continuity equation (4.1.12) in time, and elimination of velocity tendencies with the help of (4.2.1), (4.2.2) and (4.2.11), yields the η-coordinate form of elliptic equation (3.2.7):

$$\mathcal{L}\phi \equiv \hat{\mathbf{G}}^+\cdot\hat{\mathbf{G}}\phi + \frac{1}{m}\frac{\partial}{\partial\eta}\left(\frac{p^2}{mH^2}\frac{\partial\phi}{\partial\eta}\right) = A^v \ , \tag{4.2.13a}$$

where the volume-distributed source function is

$$A^v = \hat{\mathbf{G}}^+\cdot\mathbf{F_v} + \frac{1}{m}\frac{\partial F_\omega}{\partial\eta} \ , \tag{4.2.13b}$$

and $\mathbf{F_v} = \{F_u,\ F_v\}$.
The boundary conditions (3.3.4), (3.4.11), and (3.3.6) become

$$\left(\frac{\partial\phi}{\partial n}\right)_\Gamma = a_\Gamma, \tag{4.2.14}$$

$$\nabla\cdot\int_0^1(\hat{\mathbf{G}}\phi)md\eta = \nabla\cdot\int_0^1\mathbf{F_v}md\eta - \frac{\partial^2\overline{p}_0}{\partial t^2} \ , \tag{4.2.15}$$

$$\int_0^1|\phi|md\eta < \infty, \quad \text{if} \quad \int_0^1|A|md\eta < \infty. \tag{4.2.16}$$

They define the structure of the boundary-distributed singular source function, which is the same as (3.3.7)

$$A^b(\mathbf{x},\eta,t) = \gamma(\mathbf{x},t)\delta(\eta,1) + f(\mathbf{x}_\Gamma,\eta,t)\delta(\mathbf{x},\mathbf{x}_\Gamma) \ . \tag{4.2.17}$$

5 Discrete anelastic hybrid-coordinate model

Discretization takes advantage of the hydrostatic HIRLAM framework to full extent. Some minor changes are introduced into computation of the discrete thermic geopotential with the aim to increase smoothness of the source A^v, which is accompanied with alterations in energy conversion term. However, all these changes are not too extensive.

The grid is the classical staggered (Arakawa C) grid. The surfaces $i = 1/2,\ Nlon + 1/2$, and $j = 1/2,\ Nlat + 1/2$ are lateral boundaries, $k = 1/2$ corresponds to the level $\eta = 0$ (outer space) and $k = Nlev + 1/2$ corresponds to $\eta = 1$ (model surface $p = \overline{p}_0$). It is convenient to consider each small cube with the center at $\{i, j, k\}$ and facets at $\{i \pm 1/2, j, k\}$, $\{i, j \pm 1/2, k\}$, and $\{i, j, k \pm 1/2\}$, as an elementary pseudo-particle. The discrete scalar fields: temperature T, specific humidity q, etc., and baric geopotential ϕ are located in particle centers:

$$T_{ijk}, \quad \phi_{ijk}, \quad q_{ijk},$$

whereas the components of vectors u, v, ω (and $m\dot{\eta}$, w), determining in- and outflows on the particle boundaries, are located in the centers of particle facets:

$$u_{i+1/2jk}, \quad v_{ij+1/2k}, \quad \omega_{ijk+1/2}\ , \quad (m\dot{\eta})_{ijk+1/2}\ .$$

Also, the discrete pressure is located in the centers of horizontal facets:

$$p_{ijk+1/2},$$

and, consequently, the pressure difference belongs to scalars:

$$(\Delta_\eta p)_{ijk} = p_{ijk+1/2} - p_{ijk-1/2}\ .$$

Standard notation is used for averaging and difference operators, and for finite differences:

$$\overline{A}^{\xi}_{l} = \frac{A_{l-1/2} + A_{l+1/2}}{2}\ , \quad \overline{A}^{\xi}_{l+1/2} = \frac{A_l + A_{i+1}}{2}\ ,$$

$$(\delta_\xi A)_l = \frac{A_{l+1/2} - A_{l-1/2}}{\xi_{l+1/2} - \xi_{l-1/2}}\ , \quad (\delta_\xi A)_{l+1/2} = \frac{A_{l+1} - A_l}{\xi_{l+1} - \xi_l}\ ,$$

$$(\Delta_\xi A)_l = A_{l+1/2} - A_{l-1/2}\ , \quad (\Delta_\xi A)_{l+1/2} = A_{l+1} - A_l\ ,$$

where ξ is for x, y, or η.

Horizontal averaging over the kth η-level is denoted as

$$\langle a \rangle_k = \frac{1}{NlonNlat} \sum_{ij} a_{ijk} \ .$$

5.1 Diagnostics

The pressure is

$$p_{ijk+1/2} = A_{k+1/2} + B_{k+1/2} \overline{p}_{0ij} \ , \tag{5.1.1}$$

where

$$A_{k+1/2} \ = \ A(\eta_{k+1/2}) \ , \quad B_{k+1/2} \ = \ B(\eta_{k+1/2}) \ , \tag{5.1.2a}$$

$$A_{1/2} \ = \ A_{Nlev+1/2} \ = 0 \ , \quad B_{1/2} \ = 0 \ , \quad B_{Nlev+1/2} = 1 \ . \tag{5.1.2b}$$

The coordinate differences are $\Delta x = a\Delta\lambda$, $\Delta y = a\Delta\theta$, $\Delta\eta$. The physical differences along the horizontal coordinate axes are

$$\Delta X_{ij} = h_{xij}\Delta x \ , \quad \Delta Y_{ij} = h_{yij}\Delta y \ . \tag{5.1.3}$$

The horizontal divergence, a finite-difference analogue of (4.1.7), is

$$(\nabla \cdot \mathbf{a})_{ijk} = \frac{1}{(h_x h_y)_{ij}} \left[\delta_x (\overline{h_y}^x a_x) + \delta_y (\overline{h_x}^y a_y) \right]_{ijk} \ , \tag{5.1.4}$$

whereas the horizontal gradient of a scalar a_{ijk} has components

$$[(\nabla a)_x]_{i+1/2jk} = \frac{1}{h_{xi+1/2j}} (\delta_x a)_{i+1/2jk} = \frac{a_{i+1jk} - a_{ijk}}{h_{xi+1/2j}\Delta x} \ , \tag{5.1.5a}$$

$$[(\nabla a)_y]_{ij+1/2k} = \frac{1}{h_{yij+1/2}} (\delta_y a)_{ij+1/2k} = \frac{a_{ij+1k} - a_{ijk}}{h_{yij+1/2}\Delta y} \ . \tag{5.1.5b}$$

In these difference formulae we have maintained the original, formal, two-dimensional structure of h_x and h_y, used in HIRLAM (both for better coincidence with the HIRLAM formalism and for larger symmetry), though actually $h_{xij} \ = \ h_{xj}$ depends on the meridional index only, whereas $h_{yij} \ = \ 1$. The auxiliary vector $\mathbf{V} = \{U_{i+1/2jk}, V_{ij+1/2k}\}$ is:

$$U_{i+1/2jk} = (\overline{\Delta_\eta p}^x u)_{i+1/2jk} \ , \quad V_{ij+1/2k} = \left(\overline{\Delta_\eta p}^y u\right)_{ij+1/2k} \ . \tag{5.1.6}$$

The discrete analogue of (4.1.11) will then be

$$(m\dot{\eta})_{ijk+1/2} = (1 - B_{k+1/2})\frac{\partial \overline{p}_0}{\partial t} + \sum_{k'=k+1}^{Nlev} (\nabla \cdot \mathbf{V})_{ijk'} \ , \tag{5.1.7}$$

from which the recurrence formula (the discrete form of (4.1.6)) follows

$$(m\dot{\eta})_{ijk-1/2} = (m\dot{\eta})_{ijk+1/2} + (\nabla \cdot \mathbf{V})_{ijk} + \Delta B_k \frac{\partial \overline{p}_{0ij}}{\partial t} \ , \tag{5.1.8a}$$

$$(m\dot{\eta})_{ijNlev+1/2} = 0 \ . \tag{5.1.8b}$$

The vertically integrated mass balance condition (4.1.10) becomes

$$\frac{\partial \overline{p}_{0ij}}{\partial t} + \sum_{k=1}^{Nlev} (\nabla \cdot \mathbf{V})_{ijk} \ = \ 0 \ . \tag{5.1.9}$$

The formula (4.1.8') for omega-velocity is

$$\omega_{ijk+1/2} = (m\dot{\eta})_{ijk+1/2} + (\overline{\mathbf{v}}^{\eta} \cdot \nabla p)_{ijk+1/2} + \frac{\partial p_{ijk+1/2}}{\partial t} \ , \tag{5.1.10}$$

where we define

$$(\overline{\mathbf{v}}^{\eta} \cdot \nabla p)_{ijk+1/2} \equiv \frac{1}{(h_x h_y)_{ij}} \left(\overline{\overline{h_y}^{x} \overline{u}^{\eta} \delta_x p}^{x} + \overline{\overline{h_x}^{y} \overline{v}^{\eta} \delta_y p}^{y} \right)_{ijk+1/2} \ . \tag{5.1.11}$$

For the operator $\hat{\mathbf{G}}^{+}$ a discrete presentation follows from these definitions

$$(\hat{\mathbf{G}}^{+} \cdot \mathbf{v})_{ijk} = \frac{[\nabla \cdot \mathbf{V} - \Delta_{\eta}(\overline{\mathbf{v}}^{\eta} \cdot \nabla p)]_{ijk}}{(\Delta_{\eta} p)_{ijk}}$$

$$= \frac{1}{(\Delta_{\eta} p h_x h_y)_{ijk}} \left[\delta_x \left(\overline{h_y}^{x} \overline{\Delta_{\eta} p}^{x} u \right) - \Delta_{\eta} \left(\overline{\overline{h_y}^{x} \overline{u}^{\eta} \delta_x p}^{x} \right) \right]_{ijk}$$

$$+ \frac{1}{(\Delta_{\eta} p h_x h_y)_{ijk}} \left[\delta_y \left(\overline{h_x}^{y} \overline{\Delta_{\eta} p}^{y} v \right) - \Delta_{\eta} \left(\overline{\overline{h_x}^{y} \overline{v}^{\eta} \delta_y p}^{y} \right) \right]_{ijk} \ . \tag{5.1.12}$$

This formula can be simplified (Appendix A) to

$$(\hat{\mathbf{G}}^{+} \cdot \mathbf{v})_{ijk} = \frac{1}{(h_x h_y)_{ij}} \left[\delta_x (\overline{h_y}^{x} u) - \frac{\overline{\overline{h_y}^{x} (\Delta_{\eta} u) \delta_x p}^{x\eta}}{\Delta_{\eta} p} + \delta_y (\overline{h_x}^{y} v) - \frac{\overline{\overline{h_x}^{y} (\Delta_{\eta} v) \delta_y p}^{y\eta}}{\Delta_{\eta} p} \right]_{ijk} \ , \tag{5.1.12'}$$

which is a discrete analogue for (4.1.13'). The conjugated to (5.1.12) gradient is (for details see Appendix A)

$$(\hat{G}_x\phi)_{i+1/2jk} = \frac{1}{\overline{h_x}^x}\left[\delta_x\phi - \frac{\overline{(\delta_x p)\Delta_\eta\overline{\phi}^{x\eta}}}{\overline{\Delta_\eta p}^x}\right]_{i+1/2jk} , \qquad (5.1.13a)$$

$$(\hat{G}_y\phi)_{ij+1/2k} = \frac{1}{\overline{h_y}^y}\left[\delta_y\phi - \frac{\overline{(\delta_y p)\Delta_\eta\overline{\phi}^{y\eta}}}{\overline{\Delta_\eta p}^y}\right]_{ij+1/2k} . \qquad (5.1.13b)$$

The discrete analogue of (4.1.12), consistent with (5.1.8) - (5.1.12), is

$$\left(\hat{\mathbf{G}}^+\cdot\mathbf{v} + \frac{\Delta_\eta\omega}{\Delta_\eta p}\right)_{ijk} = 0 . \qquad (5.1.14)$$

The thermic geopotential (4.2.10) is

$$\varphi_{ijk-1/2} = gh_{ij} + \sum_{k'=k}^{Nlev}(RT)_{ijk'}\alpha_{ijk'} , \qquad (5.1.15)$$

where

$$\alpha_{ijk} = (\Delta_\eta \ln p)_{ijk} = \ln p_{ijk+1/2} - \ln p_{ijk-1/2} , \; k \neq 1, \quad \text{and} \quad \alpha_{ij1} = 2\ln 2 . \qquad (5.1.16)$$

The thermic geopotential can be evaluated also from the recurrence

$$\begin{aligned} \varphi_{ijNlev+1/2} &= gh_{ij} , \\ \overline{\varphi}^\eta_{ijk} &= \varphi_{ijk+1/2} + \frac{1}{2}(RT)_{ijk}\alpha_{ijk} , \\ \varphi_{ijk-1/2} &= \overline{\varphi}^\eta_{ijk} + \frac{1}{2}(RT)_{ijk}\alpha_{ijk} . \end{aligned} \qquad (5.1.17)$$

Coefficients α_{ijk} are different from those, employed in the common hydrostatic HIRLAM, and thus, the thermic geopotential diagnostics is different. Such a modification is required for reduction of numerical noise at the computation of the divergence $\hat{\mathbf{G}}^+\cdot(\hat{\mathbf{G}}\varphi)$, which constitutes a major contribution to the source A^v in the elliptic equation (4.2.13).

5.2 Dynamics

The equations of motion (4.2.1) – (4.2.3) are in the discrete model

$$\left(\frac{u^{t+\Delta t}-u^{t-\Delta t}}{2\Delta t}\right)_{i+1/2jk} = F_{ui+1/2jk} - (\widehat{G}_x\phi)_{i+1/2jk} \ , \tag{5.2.1}$$

$$\left(\frac{v^{t+\Delta t}-v^{t-\Delta t}}{2\Delta t}\right)_{ij+1/2k} = F_{vij+1/2k} - (\widehat{G}_y\phi)_{i+1/2jk} \ , \tag{5.2.2}$$

$$\left(\frac{T^{t+\Delta t}-T^{t-\Delta t}}{2\Delta t}\right)_{ijk} = F_{Tijk} \ . \tag{5.2.3}$$

The components of the hydrostatic velocity tendency correspond to the time level t:

$$F_{ui+1/2jk} = -\left[\frac{1}{\overline{\overline{h_x}^x}}\left(-\overline{Z\overline{\overline{h_x}^y V}^x}^y + \delta_x E + \frac{\overline{\overline{h_x m\dot{\eta}}^x \Delta_\eta u}^\eta}{\overline{\Delta_\eta p}^x}\right)\right]_{i+1/2jk}$$

$$-(\widetilde{G}_x\overline{\varphi}^\eta)_{i+1/2jk} + (P_u + K_u)_{i+1/2jk} \ , \tag{5.2.4}$$

$$F_{vij+1/2k} = -\left[\frac{1}{\overline{\overline{h_y}^y}}\left(\overline{Z\overline{\overline{h_y}^x U}^x}^y + \delta_y E + \frac{\overline{\overline{h_y m\dot{\eta}}^y \Delta_\eta v}^\eta}{\overline{\Delta_\eta p}^y}\right)\right]_{ij+1/2k}$$

$$-(\widetilde{G}_y\overline{\varphi}^\eta)_{ij+1/2k} + (P_v + K_v)_{ij+1/2k} \ , \tag{5.2.5}$$

where

$$Z_{i+1/2j+1/2k} = \frac{\left[\overline{fh_xh_y}^{xy} + \delta_x(\overline{h_y}^y v) - \delta_y(\overline{h_x}^x u)\right]_{i+1/2j+1/2k}}{(\overline{h_xh_y\Delta_\eta p}^{xy})_{i+1/2j+1/2k}} \tag{5.2.6}$$

$$E_{ijk} = \frac{1}{2}\left(\frac{1}{h_y}\overline{\overline{h_y}^x u^2}^x + \frac{1}{h_x}\overline{\overline{h_x}^y v^2}^y\right)_{ijk} \ , \tag{5.2.7}$$

and

$$(\widetilde{G}_x\overline{\varphi}^\eta)_{i+1/2jk} = \frac{1}{\overline{\overline{h_x}^x}}\left[\delta_x\overline{\varphi}^\eta - \frac{\delta_x\overline{p}^\eta\Delta_\eta\overline{\varphi}^x}{\overline{\Delta_\eta p}^x}\right]_{i+1/2jk} \ . \tag{5.2.8a}$$

$$(\widetilde{G}_x\overline{\varphi}^\eta)_{ij+1/2k} = \frac{1}{\overline{\overline{h_y}^y}}\left[\delta_y\overline{\varphi}^\eta - \frac{\delta_y\overline{p}^\eta\Delta_\eta\overline{\varphi}^y}{\overline{\Delta_\eta p}^y}\right]_{ij+1/2k} \ . \tag{5.2.8b}$$

The temperature tendency is

$$F_{Tijk} = -(\hat{a}T)_{ijk} + \left(\frac{\varkappa T\omega}{p}\right)_{ijk} + (P_T + K_T)_{ijk} \ , \tag{5.2.9}$$

where

$$(\hat{a}T)_{ijk} = \frac{[\overline{h_y U\delta_x T}^x + \overline{h_x V\delta_y T}^y + h_x h_y \overline{(m\dot{\eta})\Delta_\eta T}^\eta]_{ijk}}{(h_x h_y \Delta_\eta p)_{ijk}} \tag{5.2.10}$$

is the discrete temperature-advection term, and P_{xijk}, K_{xijk} are tendencies from physical parametrization and horizontal diffusion.

Note that the horizontal gradient $\widetilde{\mathbf{G}}$ in (5.2.8) is different from $\hat{\mathbf{G}}$, defined in (5.1.13). The modification consists in the substitution of terms $\overline{\delta_x p \Delta_\eta \overline{\varphi}^{\eta\lambda}}^\eta$ and $\overline{\delta_y p \Delta_\eta \overline{\varphi}^{\eta\theta}}^\eta$, including double vertical averaging, by more simple, vertically diagonal approximations $\delta_x \overline{p}^\eta \Delta_\eta \overline{\varphi}^x$ and $\delta_y \overline{p}^\eta \Delta_\eta \overline{\varphi}^y$. Such modification gives rise to the numerical smoothness of this term, which is substantial at high resolutions in the steep orography case.

The discrete presentation of the energy conversion term in (5.2.9) is

$$\left(\frac{RT\omega}{p}\right)_{ijk} = -\left(\Omega \frac{\Delta_\eta \varphi}{\Delta_\eta p}\right)_{ijk} \ , \tag{5.2.11a}$$

where

$$\Omega_{ijk} = \overline{\omega}^\eta_{ijk} - \left[\frac{\overline{\overline{h_y}^x \Delta_\eta \left(\delta_x p \Delta_\eta u\right)}^x + \overline{\overline{h_x}^y \Delta_\eta \left(\delta_y p \Delta_\eta v\right)}^y}{4 h_y h_x}\right]_{ijk} \ . \tag{5.2.11b}$$

This formula is consistent with the discrete presentation of the thermic geopotential (5.1.15) and definition (5.2.8), which is proved in Appendix B (see (B.5)), where the overall energetics of the discrete model is checked. The term in the square brackets is caused by the use of approximation (5.2.8) instead of (5.1.13). This term is a second order small quantity as it is proportional to a second order vertical difference and tends to zero like $(\Delta_\eta p)^2$. Except for very poor vertical resolution or drastic variations of the horizontal wind with height, it can be omitted and the energy conversion term can be simplified to

$$\left(\frac{\varkappa T\omega}{p}\right)_{ijk} = \overline{\omega}^\eta_{ijk} \frac{(\varkappa T\alpha)_{ijk}}{(\Delta_\eta p)_{ijk}} \ . \tag{5.2.11$'$}$$

5.3 The elliptic equation for baric geopotential

For establishment of the proper form of elliptic equation we also need the discrete analogue of the omega-equation (4.2.11) - (4.2.12). Proceeding from energy conservation, it is correct to start from the definition

$$\omega_{ijk+1/2} = -\left(\frac{w^s p}{\overline{\overline{H}^{\eta}}}\right)_{ijk+1/2} , \tag{5.3.1}$$

where $w^s_{ijk+1/2}$ is the hydrostatic vertical velocity, which does make use of the tendency equation (comes from (3.1.2) with the help of (2.2.1') and (3.2.1))

$$\left(\frac{w^{st+\Delta t} - w^{st-\Delta t}}{2\Delta t}\right)_{ijk+1/2} = \left(\frac{p}{\overline{H}^{\eta}}\frac{\Delta_\eta \phi}{\overline{\Delta_\eta p}^{\eta}}\right)_{ijk+1/2}$$

$$-(\hat{a}w^s)_{ijk+1/2} + (P_w + K_w)_{ijk+1/2} , \tag{5.3.2a}$$

with $\hat{a}w^s$ representing the transport of vertical velocity

$$(\hat{a}w^s)_{ijk+1/2} = \frac{[\overline{h_y \overline{U}^{\eta}\delta_x w^s}^{x} + \overline{h_x \overline{V}^{\eta}\delta_y w^s}^{y} + h_x h_y \overline{\overline{m\dot{\eta}}^{\eta}\Delta_\eta w^s}^{\eta}]_{ijk+1/2}}{(h_x h_y \overline{\Delta_\eta p}^{\eta})_{ijk+1/2}} , \tag{5.3.2b}$$

and P_w and K_w representing the physical parametrization and spectral diffusion terms for w^s. The correspondence of (5.3.2) to energy conservation is established in Appendix B.

Differentiation of (5.3.1) in time gives

$$\left(\frac{\omega^{t+\Delta t} - \omega^{t-\Delta t}}{2\Delta t}\right)_{ijk+1/2} = F_{\omega ijk+1/2} - \left[\left(\frac{p}{\overline{H}^{\eta}}\right)^2 \frac{\Delta_\eta \phi}{\overline{\Delta_\eta p}^{\eta}}\right]_{ijk+1/2} , \tag{5.3.3a}$$

where

$$F_{\omega ijk+1/2} = \left[\frac{p}{\overline{H}^{\eta}}(\hat{a}w^s - K_w - P_w)\right]_{ijk+1/2} + \left(\frac{\omega}{\overline{T}^{\eta}}\overline{F_T}^{\eta}\right)_{ijk+1/2} . \tag{5.3.3b}$$

Differentiation of the discrete continuity equation (5.1.14) in time, and elimination of the velocity tendencies with the help of (5.2.1), (5.2.2), and (5.3.3) yields the discrete form of elliptic equation:

$$(\mathcal{L}\phi)_{ijk} = A^v_{ijk} ,$$

where the discrete elliptic operator is

$$(\mathcal{L}\phi)_{ijk} = (\hat{\mathbf{G}}^{+} \cdot \hat{\mathbf{G}}\phi)_{ijk} + \left[\frac{1}{\Delta_\eta p}\Delta_\eta \left(\frac{p^2}{(\overline{H}^{\eta})^2}\frac{\Delta_\eta \phi}{\overline{\Delta_\eta p}^{\eta}}\right)\right]_{ijk} , \qquad (5.3.4a)$$

and the volume-distributed source function is

$$A^{v}_{jik} = (\hat{\mathbf{G}}^{+} \cdot \mathbf{F_v})_{ijk} + \left(\frac{\Delta_\eta F_\omega}{\Delta_\eta p}\right)_{ijk} . \qquad (5.3.4b)$$

Here $\mathbf{F_v} = \{F_{ui+1/2jk},\ F_{vij+1/2k}\}$. Keeping in mind a solution of this equation in the orthogonal basis, we will supplement the source function with a singular, boundary-distributed source A^b, and consider the equation in the form

$$(\mathcal{L}\phi)_{ijk} = A_{ijk} , \qquad (5.3.4c)$$

where

$$A_{\phi ijk} = A^{v}_{jik} + A^{b}_{ijk} . \qquad (5.3.4d)$$

The boundary-distributed source function is a discrete analogue of (4.2.17)

$$A^{b}_{jik} = f^{xl}_{jk} c^x \delta_{i,1} - f^{xr}_{jk} c^x \delta_{i,Nlon} + f^{yl}_{ik} c^y \delta_{j,1} - f^{yr}_{ik} c^y \delta_{j,Nlat} + \gamma_{ij}\delta_{k,Nlev} , \qquad (5.3.4e)$$

where

$$c^x = \frac{2}{\langle h_x \rangle \Delta x} , \qquad d^y = \frac{2}{\langle h_y \rangle \Delta y}$$

and $\delta_{i,j}$ is the Kronecker symbol. Note that functions $c^x\delta_{i,i'}$, $c^y\delta_{j,j'}$ represent the discrete analogues of the Dirac delta-function $\delta(\mathbf{x}, \mathbf{x_\Gamma})$ on the x- and y-walls, respectively.

The amplitudes of lateral sources f and bottom source γ are determined by nonhomogeneous lateral conditions, and vertical condition, respectively.

5.3.1 Boundary conditions for the elliptic equation

The **condition of integrability** (4.2.16) reduces in the discrete case to a requirement that the solution has no rapidly (exponentially) increasing mode at $k \to 0$. This is achieved, employing the eigenfunction technique in η–coordinate.

The **vertical condition** (mass balance condition for ϕ), a discrete analogue of (4.2.15), follows, differentiating (5.1.9) in time and eliminating the velocity tendencies with the help of (5.2.1) and (5.2.2)

$$(\hat{B}\phi)_{ij} \equiv \sum_{k=1}^{Nlev} \left[\delta_x \left(\overline{h_y}^x \overline{\Delta_\eta p}^x \hat{G}_x \phi \right) + \delta_y \left(\overline{h_x}^y \overline{\Delta_\eta p}^y \hat{G}_y \phi \right) \right]_{ijk} = b_{ij} \ , \quad (5.3.5a)$$

$$b_{ij} = \sum_{k=1}^{Nlev} \left[\delta_x \left(\overline{h_y}^x \overline{\Delta_\eta p}^x \hat{F}_u \right) + \delta_y \left(\overline{h_x}^y \overline{\Delta_\eta p}^y \hat{F}_v \right) \right]_{ijk} + \frac{\partial^2 \overline{p}_{0ij}}{\partial t^2} \ . \quad (5.3.5b)$$

This condition is used for the specification of coefficients γ_{ij} in the boundary source (5.3.4e).

The **lateral boundary condition** (4.2.14) becomes in the discrete case

$$\left(\frac{1}{\overline{h_x}^x} \delta_x \phi \right)_{3/2,jk} = a^{xl}_{jk} \ , \quad \left(\frac{1}{\overline{h_x}^x} \delta_x \phi \right)_{Nlon-1/2,jk} = a^{xr}_{jk} \ , \quad (5.3.6a)$$

$$\left(\frac{1}{\overline{h_y}^y} \delta_y \phi \right)_{i,3/2,k} = a^{yl}_{ik} \ , \quad \left(\frac{1}{\overline{h_y}^y} \delta_y \phi \right)_{i,Nlat-/2,k} = a^{yr}_{ik} \ , \quad (5.3.6b)$$

where coefficients a are known. These conditions will determine the coefficients f in the boundary source (5.3.4e).

In a particular case of smooth (along boundary) a and large $Nlon$, $Nlat$, $Nlev$, coefficients f in (5.3.4e) are related to the boundary gradients explicitly (Appendix D)

$$f^{xl}_{jk} = a^{xl}_{jk} \ , f^{xr}_{jk} = a^{xr}_{jk} \ , f^{yl}_{ik} = a^{yl}_{ik} \ , f^{yr}_{ik} = a^{yr}_{ik} \ . \quad (5.3.7)$$

Consequently, the boundary source (5.3.4e) transforms in the continuous limit to (4.2.17) with

$$f(\mathrm{x}_\Gamma, \eta, t) = -a_\Gamma \ , \quad (5.3.7')$$

where a_Γ represents the given normal boundary gradient of ϕ (see (3.3.4)).

5.3.2 Solver for the elliptic equation

The general idea is to solve the equation (5.3.4c) in the tree-dimensional orthogonal basis for given A^v and for A^b with optional coefficients f and γ, and then determine coefficients γ from (5.3.5), and f from (5.3.6). For application

of the basis in all three coordinates, equation (5.3.4) and condition (5.3.5) have to be represented as the sums of horizontally homogeneous main parts and horizontally nonhomogeneous perturbations. The main elliptic operator is inverted explicitly, then the solution is substituted into the perturbation terms and a new improved solution is looked for, repeating the procedure until the required precision is achieved. As the metric coefficient h_x depends on the spherical Earth in the latitude θ, the planet's roundness is considered in this algorithm as a perturbation to the plane geometry. This means that too large areas will not be accessible by the model. In practice, integration areas are limited within a square with 5 000 km long side.

Equation (5.3.4c) is presented as

$$(\overline{\mathcal{L}}\phi)_{ijk} = A_{ijk} - (\mathcal{L}'\phi)_{ijk} \ , \tag{5.3.8}$$

where

$$(\overline{\mathcal{L}}\phi)_{ijk} = (\mathcal{L}_x\phi)_{ijk} + (\mathcal{L}_y\phi)_{ijk} + (\mathcal{L}_\eta\phi)_{ijk} \ , \tag{5.3.9a}$$

$\mathcal{L}_x$,$\mathcal{L}_y$, and $\mathcal{L}_\eta$ are the horizontally homogenized, one-dimensional Laplacians

$$(\mathcal{L}_x\phi)_{ijk} = \left(\frac{1}{\langle h_x\rangle}\delta_x\phi\right)^2_{ijk} \ , \quad (\mathcal{L}_x\phi)_{ijk} = \left(\frac{1}{\langle h_y\rangle}\delta_y\phi\right)^2_{ijk} \tag{5.3.9b}$$

$$(\mathcal{L}_\eta\phi)_{ijk} \ = \left[\frac{1}{\langle\Delta_\eta p\rangle}\Delta_\eta\left(\frac{\langle p\rangle^2}{\langle\overline{H}^\eta\rangle^2}\frac{\Delta_\eta\phi}{\Delta_\eta\overline{p}^\eta}\right)\right]_{ijk} \ , \tag{5.3.9c}$$

and $\mathcal{L}'$ is defined as

$$\mathcal{L}' = \mathcal{L} - \overline{\mathcal{L}} \ . \tag{5.3.9d}$$

Analogical expansion of the integral condition (5.3.5) to the sum of main and perturbation parts gives

$$(\hat{B}^0\phi)_{ij} = b_{ij} - (\hat{B}'\phi)_{ij} \ , \tag{5.3.10a}$$

where $\hat{B}^0$ is the horizontally homogenized part of $\hat{B}$

$$(\hat{B}^0\phi)_{ij} = \langle h_x\rangle\langle h_y\rangle\left[(\mathcal{L}_x + \mathcal{L}_y)\sum_{k=1}^{Nlev}\langle\Delta_\eta p\rangle_k\phi_k\right]_{ij} \tag{5.3.10b}$$

and perturbation $\hat{B}'$ is defined as

$$(\hat{B}'\phi)_{ij} = (\hat{B}\phi)_{ij} - (\hat{B}^0\phi)_{ij} \ . \tag{5.3.10c}$$

The iterative algorithm is

$$\phi^{(0)}_{ijk} = 0 \ \text{ at } \ t = 0, \quad \text{ and } \ [\phi^{(0)}_{ijk}]^t = [\phi^{(final)}_{ijk}]^{t-\Delta t} \ \text{ at } \ t > 0, \qquad (5.3.11a)$$

and for l = 1,2,....

$$(\overline{\mathcal{L}}\phi^{(l)})_{ijk} = A^v_{ijk} + A^{b(l)}_{ijk} - (\mathcal{L}'\phi^{(l-1)})_{ijk} \ \equiv \ \mathcal{A}^{(l)}_{ijk}, \qquad (5.3.11b)$$

$$(\hat{B}^0\phi^{(l)})_{ij} = b_{ij} - (\hat{B}'\phi^{(l-1)})_{ij} \equiv b^{(l)}_{ij} \ , \qquad (5.3.11c)$$

where $A^{b(l)}$ is the iterated boundary source

$$A^{b(l)}_{jik} = f^{xl(l)}_{jk} c^x \delta_{i,1} - f^{xr(l)}_{jk} c^x \delta_{i,Nlon} + f^{yl(l)}_{ik} c^y \delta_{j,1} - f^{yr(l)}_{ik} c^y \delta_{j,Nlat} + \gamma^{(l)}_{ij} \delta_{k,Nlev} \qquad (5.3.11d)$$

with the iterated coefficients $f^{(l)}$, $\gamma^{(l)}$, which have to be specified from the iterated versions of conditions (5.3.6):

$$\left(\frac{1}{\overline{h_x}^x}\delta_x\phi^{(l)}\right)_{3/2,jk} = a^{xl}_{jk} \ , \quad \left(\frac{1}{\overline{h_x}^x}\delta_x\phi^{(l)}\right)_{Nlon-1/2,jk} = a^{xr}_{jk} \ , \qquad (5.3.11e)$$

$$\left(\frac{1}{\overline{h_y}^y}\delta_y\phi^{(l)}\right)_{i,3/2,k} = a^{yl}_{ik} \ , \quad \left(\frac{1}{\overline{h_y}^y}\delta_y\phi^{(l)}\right)_{i,Nlat-/2,k} = a^{yr}_{ik} \ , \qquad (5.3.11f)$$

and from (5.3.11c), respectively.

The iterative set of equations (5.3.11) is solved using the three-dimensional orthogonal basis $X \otimes Y \otimes E$, where

$$X = \{X_q, q = 1, .., Nlon\} = \{\{X_{iq}, i = 1..., Nlon\}, q = 1, ..., Nlon\} \ ,$$

$$Y = \{Y_r, r = 1, .., Nlat\} Y_r = \{\{Y_{jr}, j = 1..., Nlat\}, r = 1, ..., Nlat\} \ ,$$

$$E = \{E_s, s = 1, .., Nlev\} E_s = \{\{E_{ks}, k = 1..., Nlev\}, s = 1, ..., Nlev\} \ ,$$

represent the one-dimensional bases in the x, y and η dimensions, respectively. They are chosen as the eigenvectors of the one-dimensional Laplacians:

$$(\mathcal{L}_x X_q)_i = -\lambda^x_q X_{iq} \ , \quad (\mathcal{L}_y Y_r)_j = -\lambda^y_r Y_{jr} \ , \quad (\mathcal{L}_\eta E_s)_k = -\lambda^\eta_s E_{ks} \ , \qquad (5.3.12)$$

where λ^x_q, λ^y_r, λ^η_s are the corresponding eigenvalues.

For X and Y the discrete normalized cosine bases are employed (see Appendix C), whereas the basis E and eigenvalues λ^η (they depend on the vertical temperature distribution in the atmosphere) are specified, numerically solving the vertical eigenvalue problem (*ibid*).

Presenting $\phi^{(l)}$ in the basis

$$\phi^{(l)}_{ijk} = \sum_{qrs} X_{iq} Y_{jr} E_{ks} \tilde{\phi}^{(l)}_{qrs} \ , \tag{5.3.13}$$

the solution of the equation (5.3.11b) for Fourier coefficients $\tilde{\phi}$ will be

$$\tilde{\phi}^{(l)}_{qrs} = -\frac{\tilde{\mathcal{A}}^{(l)}_{qrs}}{\lambda^x_q + \lambda^y_r + \lambda^\eta_s} \ , \tag{5.3.14a}$$

$$\tilde{\mathcal{A}}^{(l)}_{qrs} = \tilde{A}^v_{qrs} - (\widetilde{\mathcal{L}'\phi^{(l-1)}})_{qrs} +$$

$$c^x \tilde{f^{xl}_{rs}}^{(l)} X_{q,1} - c^x \tilde{f^{xr}_{rs}}^{(l)} X_{q,Nlon} + c^y \tilde{f^{yl}_{qs}}^{(l)} Y_{r,1} - c^y \tilde{f^{yr}_{qs}}^{(l)} Y_{r,Nlat} + \tilde{\gamma}^{(l)}_{qr} E^{-1}_{s,Klev}, \tag{5.3.14b}$$

where $\tilde{\mathcal{A}}^v$, $\widetilde{\mathcal{L}'\phi^{(l-1)}}$ are the Fourier coefficients of the volume distributed source and perturbation term

$$\tilde{A}^v_{qrs} = \sum_{ijk} X_{qi} X_{rj} E^{-1}_{sk} \mathcal{A}^v_{ijk} \ , \quad (\widetilde{\mathcal{L}'\phi^{(l-1)}})_{qrs} = \sum_{ijk} X_{qi} X_{rj} E^{-1}_{sk} (\mathcal{L}'\phi^{(l-1)})_{qrs} \ ,$$

and $\tilde{f}^{(l)}$, $\tilde{\gamma}^{(l)}$ are the Fourier coefficients of $f^{(l)}$, $\gamma^{(l)}$:

$$\tilde{f}^{xl/r(l)}_{rs} = \sum_{jk} Y_{rj} E^{-1}_{sk} f^{xl/r(l)}_{jk}, \ \tilde{f}^{yl/r(l)}_{qs} = \sum_{ik} X_{qi} E^{-1}_{sk} f^{yl/r(l)}_{ik}, \ \tilde{\gamma}^{(l)}_{qr} = \sum_{ij} X_{qi} Y_{rj} \gamma^{(l)}_{ij}.$$

Substitution of the solution (5.3.14) into the boundary conditions (5.3.11e) - (5.3.11f) yields (for details see Appendix D) an iterative algorithm for the Fourier coefficients of the boundary force:

$$\tilde{f^{xl}_{rs}}^{(l)} = \tilde{f^{xl}_{rs}}^{(l-1)} + \delta \tilde{f^{xl}_{rs}}^{(l)} \ , \tag{5.3.15a}$$

$$\tilde{f^{xr}_{rs}}^{(l)} = \tilde{f^{xr}_{rs}}^{(l-1)} + \delta \tilde{f^{xr}_{rs}}^{(l)} \ , \tag{5.3.15b}$$

$$\tilde{f^{yl}_{qs}}^{(l)} = \tilde{f^{yl}_{qs}}^{(l-1)} + \delta \tilde{f^{yl}_{qs}}^{(l)} \ , \tag{5.3.15c}$$

$$f^{\tilde{y}r\,(l)}_{qs} = f^{\tilde{y}r\,(l-1)}_{qs} + \delta f^{\tilde{y}r\,(l)}_{qs} \ , \qquad (5.3.15d)$$

where the increments are

$$\delta \tilde{f}^{xl(l)}_{rs} = \frac{1}{s^x_{rs}} \left[\tilde{a}^{xl}_{rs} - \left(\widetilde{\frac{1}{h_x} \delta_x \phi^{(l-1)}} \right)_{3/2,r,s} \right] \ , \qquad (5.3.16a)$$

$$\delta \tilde{f}^{xr(l)}_{rs} = \frac{1}{s^x_{rs}} \left[\tilde{a}^{xr}_{rs} - \left(\widetilde{\frac{1}{h_x} \delta_x \phi^{(l-1)}} \right)_{Nlon-1/2,r,s} \right] \ , \qquad (5.3.16b)$$

$$\delta \tilde{f}^{yl(l)}_{qs} = \frac{1}{s^y_{qs}} \left[\tilde{a}^{yl}_{qs} - \left(\widetilde{\frac{1}{h_y} \delta_y \phi^{(l-1)}} \right)_{q,3/2,s} \right] \ , \qquad (5.3.16c)$$

$$\delta \tilde{f}^{yr(l)}_{qs} = \frac{1}{s^y_{qs}} \left[\tilde{a}^{yr}_{qs} - \left(\widetilde{\frac{1}{h_y} \delta_y \phi^{(l-1)}} \right)_{q,Nlat-1/2,s} \right] \ . \qquad (5.3.16d)$$

and

$$s^x_{rs} = \frac{1}{Nlon-1} \left(\sum_{q=2}^{Nlon-1} \frac{\lambda^x_q}{\lambda^x_q + \lambda^y_r + \lambda^\eta_s} + \frac{2}{(\langle h_x \rangle \Delta x)^2 (\lambda^x_{Nlon} + \lambda^y_r + \lambda^\eta_s)} \right) \ , \qquad (5.3.17a)$$

$$s^y_{qs} = \frac{1}{Nlat-1} \left(\sum_{r=2}^{Nlat-1} \frac{\lambda^y_r}{\lambda^x_q + \lambda^y_r + \lambda^\eta_s} + \frac{2}{(\langle h_y \rangle \Delta y)^2 (\lambda^x_q + \lambda^y_{Nlat} + \lambda^\eta_s)} \right) \ . \qquad (5.3.17b)$$

In the case of smooth boundary conditions and for large grids ($Nlon$, $Nlat$, $Nlev \to \infty$), the square brackets in formulae (5.3.16) become zero at $l = 2$, which yields the case (5.3.7) (Appendix D).

After the coefficients $\tilde{f}$ are specified from (5.3.15), (5.3.16), the source function (5.3.14b) still includes unknown coefficients $\tilde{\gamma}$, which can be solved from (5.3.11c). Transforming this relationship into the basis and using representation (5.3.14) (where $\tilde{f}^{(l)}$ are specified from (5.3.15)), the explicit formula for γ results

$$\tilde{\gamma}^{(l)}_{qr} = \frac{1}{s^\eta_{qr}} \left[\frac{\tilde{b}_{qr} - (\widetilde{B' \phi^{(l-1)}})_{qr}}{\langle h_x \rangle \langle h_y \rangle (\lambda^x_q + \lambda^y_r)} - \sum_s \frac{c_s A^{\gamma(l)}_{qrs}}{\lambda^x_q + \lambda^y_r + \lambda^\eta_s} \right] \ , \qquad (5.3.18a)$$

where

$$s^{\eta}_{qr} = \sum_s \frac{c_s E^{-1}_{s,lev}}{\lambda^x_q + \lambda^y_r + \lambda^{\eta}_s} \ , \qquad c_s = \sum_k \langle \Delta p \rangle_k E_{ks} \ , \tag{5.3.18b}$$

$$A^{\gamma(l)} = \tilde{A}^v_{qrs} - (\widetilde{\mathcal{L}'\phi^{(l-1)}})_{qrs} +$$

$$c^x \tilde{f^{xl}_{rs}}^{(l)} X_{q,1} - c^x \tilde{f^{xr}_{rs}}^{(l)} X_{q,Nlon} + c^y \tilde{f^{yl}_{qs}}^{(l)} Y_{r,1} - c^y \tilde{f^{yr}_{qs}}^{(l)} Y_{r,Nlat} \ . \tag{5.3.18c}$$

Thus, the solution of the elliptic equation at the lth iteration is (5.3.13), where coefficients $\tilde{\phi}$ are presented by (5.3.14), with $\tilde{f}^{(l))}$ evaluated from (5.3.15) and $\gamma^{(l)}$ from (5.3.18). The iterative' process is stopped at l, for which:

$$\langle |\phi^{(l)} - \phi^{(l-1)}| \rangle < \varepsilon \langle |\phi^{(l)}| \rangle \ , \tag{5.3.19}$$

where ε depends on the required precision (The typical value in application is $\varepsilon \sim 10^{-3} - 10^{-4}$).

5.4 Boundary and initial fields

The nonhydrostatic scheme takes advantage of the Davies' boundary relaxation scheme (Davies 1976) of hydrostatic HIRLAM. Modifications, induced by the presence of nonhydrostatic force are described in the following.

Hydrostatic evolution from the time level $t - \Delta t$ to the level $t + \Delta t$, when the boundary relaxation zone (BRZ) is present, is described by the formula (for field u, cases of v and T are similar)

$$u^{t+\Delta t} = (1-\alpha)\tilde{u}^{t+\Delta t} + \alpha u_b^{t+\Delta t} \ , \quad \tilde{u}^{t+\Delta t} = u^{t-\Delta t} + 2\Delta t F_u \ ,$$

where α is the weight function, which is zero beyond the relaxation zone, increases smoothly in the relaxation zone towards the boundary, and becomes $\alpha = 1$ on the boundary Γ. Field $\tilde{u}^{t+\Delta t}$ is the evolution of u to the level $t+\Delta t$ from the initial state $u^{t-\Delta t}$ when BRZ is absent, while F_u presents the hydrostatic tendency (5.2.4). The function $u_b^{t+\Delta t}$ presents the boundary field (which represents the surrounding environment), towards which the internal field $u^{t+\Delta t}$ is relaxed and which is always reached by $u^{t+\Delta t}$ on the boundary surface Γ. From this formula, the effective ('boundary relaxed') hydrostatic tendencies are

$$\hat{F}_u = (1-\alpha)F_u + \alpha \frac{u_b^{t+\Delta t} - u^{t-\Delta t}}{2\Delta t} \ , \tag{5.4.1a}$$

$$\hat{F}_v = (1-\alpha)F_v + \alpha\frac{v_b^{t+\Delta t} - v^{t-\Delta t}}{2\Delta t} \ , \qquad (5.4.1b)$$

$$\hat{F}_T = (1-\alpha)F_T + \alpha\frac{T_b^{t+\Delta t} - T^{t-\Delta t}}{2\Delta t} \ . \qquad (5.4.1c)$$

The corresponding modifications of the nonhydrostatic equations (5.2.1) - (5.2.3) are

$$\frac{u_{i+1/2jk}^{t+\Delta t} - u_{i+1/2jk}^{t-\Delta t}}{2\Delta t} = \hat{F}_{ui+1/2jk} - (\widehat{G}_x\phi)_{i+1/2jk} \ , \qquad (5.4.2a)$$

$$\frac{v_{ij+1/2k}^{t+\Delta t} - v_{ij+1/2k}^{t-\Delta t}}{2\Delta t} = \hat{F}_{vij+1/2k} - (\widehat{G}_y\phi)_{i+1/2jk} \ , \qquad (5.4.2b)$$

$$\frac{T_{ijk}^{t+\Delta t} - T_{ijk}^{t-\Delta t}}{2\Delta t} = \hat{F}_{Tijk} \ . \qquad (5.4.2c)$$

The BRZ is not applied to ω, and its tendency remains (5.3.3). Thanks to the inclusion of the boundary relaxation in the hydrostatic tendency, the baric geopotential ϕ takes into consideration all forces and maintains the anelastic quality of the model in the whole domain, including the relaxation zone.

To establish in (5.4.2a) and (5.4.2b) rigid conditions $u^{t+\Delta t}|_\Gamma = u_b^{t+\Delta t}$, $v^{t+\Delta t}|_\Gamma = v_b^{t+\Delta t}$, the normal gradient of ϕ has to vanish on Γ, which yields zero value for the boundary function a in (5.3.6):

$$a_{jk}^{xl} = 0 \ , a_{jk}^{xr} = 0 \ , a_{ik}^{yl} = 0 \ , a_{ik}^{yr} = 0 \ . \qquad (5.4.3)$$

Consequently, the boundary source amplitude f in (5.3.4e), (5.3.11d) becomes also zero, and the iteration algorithm (5.3.15) - (5.3.16) is not required. Thus, in the case of the Davies' relaxation scheme, the lateral boundary value problem for ϕ reduces to the homogeneous Neumann problem.

An important quality of the Davies' scheme is approximation of the singular lateral boundary source A^b (see (4.2.17)) of the continuous model (without BRZ) by the volume-distributed source A^v, which in the BRZ approaches the singular limit (4.2.17), if the depth of the BRZ tends to zero. To prove this, we will consider the volume distributed source function A^v in the BRZ near the right wall in x-direction:

$$L - d < x < L \ , \qquad L = a\Lambda$$

(Discussion is confined to this particular case. However, results would be the same at the other walls). For a sufficiently narrow BRZ, when $d \rightarrow 0$, the most rapidly changing function in the tendencies (5.4.1) is the weight function α, which gradient becomes large in the BRZ. As a result, the volume-distributed source function (5.3.4b) can be estimated from (5.4.1a) - (5.4.1b) in the BRZ as

$$A^v \approx -a \, \frac{1}{h_x}\frac{\partial \alpha}{\partial x} \qquad \text{where} \qquad a = F_u - \frac{u_b^{t+\Delta t} - u^{t-\Delta t}}{2\Delta t} \; . \tag{5.4.4}$$

At the limit $d \rightarrow 0$, α approaches the Heaviside function and, consequently,

$$\frac{1}{h_x}\frac{\partial \alpha}{\partial x} \rightarrow \delta(x, x_\Gamma),$$

whereas a tends to a_Γ in (3.3.5). Thus, A^v approaches precisely the first term of the singular boundary source (4.2.17), with $f = - \, a_\Gamma$ (see (3.3.7')) where a_Γ is determined as (3.3.5).

As seen from (5.4.4), the source A^v is specified in the boundary zone by the "hydrostatic disbalance" a. Extreme values of a should be avoided, as large a would cause large amplitude of ϕ near lateral boundaries, which would result in large normal gradients of ϕ and strong spurious tangential circulation in the boundary zone. As a is mainly driven by the boundary fields u_b, v_b, T_b and $\overline{p}_0$, the amplitude of a depends how well the boundary fields, including $\overline{p}_0$, match the hydrostatic evolution model. Especially sensitive is a to the choice of the mean surface pressure field $\overline{p}_0$.

Two main choices, requiring different approach, are as follows.

a. $\overline{p_0}(x, y, t)$ is taken, along with other boundary fields u_b, v_b, and T_b, from a coarser, hydrostatic forecast model. In this case a is always small, there would be no problem with large spurious boundary sources, and the integration scheme (5.4.2a) - (5.4.2c) supported by homogeneous conditions (5.4.3), is advantageous. In this scheme, ϕ and p_0' will represent fine, small-scale, nonhydrostatic contributions to the hydrostatic fields. The described approach is attractive because of its simplicity, and it is presently applied as the basic scheme in NH HIRLAM.

b. $\overline{p_0} = \hat{p}_0(x, y)$, where $\hat{p}_0(x, y)$ is the mean barometric background pressure (2.5.7c). This approach assumes prior specification of the mean temperature $T_0(p)$. For given initial velocity and temperature fields, $\hat{p}_0$ is rather different

from the actual hydrostatic surface pressure. Consequently, the thermic and Coriolis forces are mutually out of balance, hydrostatic tendency becomes large everywhere and a in (5.4.4) becomes also large. To restore the approximate geostrophic balance in the BRZ, a compensating baric geopotential forcing must be added to the hydrostatic tendency **before the BRZ is applied**. The algorithm here is as follows. The baric geopotential is presented as a sum of the steady field ϕ_c and transient component ϕ'

$$\phi = \phi_c + \phi' \ . \tag{5.4.5}$$

The steady component is specified as a solution of the elliptic equation (5.3.4) in the homogeneous case, $a = 0$, nonhomogeneous boundary conditions

$$a^{xl}_{jk} = F_{u,3/2,j,k} \ , a^{xr}_{jk} = F_{u,Nlon-1/2,j,k} \ , a^{yl}_{ik} = F_{v,i,3/2,k} \ , a^{yr}_{ik} = F_{v,i,Nlat-1/2,k} \ , \tag{5.4.6}$$

corresponding to the actual hydrostatic tendency $\mathbf{F_v}$ on the boundary. The forcing $-\hat{\mathbf{G}}\phi_c$ is then added to the hydrostatic tendency with the resulting equations of motion

$$\frac{u^{t+\Delta t}_{i+1/2jk} - u^{t-\Delta t}_{i+1/2jk}}{2\Delta t} = \hat{F}_{ui+1/2jk} - (\widehat{G}_x\phi')_{i+1/2jk} \ , \tag{5.4.7a}$$

$$\frac{v^{t+\Delta t}_{ij+1/2k} - v^{t-\Delta t}_{ij+1/2k}}{2\Delta t} = \hat{F}_{vij+1/2k} - (\widehat{G}_y\phi')_{i+1/2jk} \ , \tag{5.4.7b}$$

where

$$\hat{F}_u = (1-\alpha)(F_u - \widehat{G}_x\phi_c) + \alpha\frac{u^{t+\Delta t}_b - u^{t-\Delta t}}{2\Delta t} \ , \tag{5.4.7c}$$

$$\hat{F}_v = (1-\alpha)(F_v - \widehat{G}_y\phi_c) + \alpha\frac{v^{t+\Delta t}_b - v^{t-\Delta t}}{2\Delta t} \ . \tag{5.4.7d}$$

The transient component ϕ' is computed at each t from the elliptic equation (5.3.4) with A, corresponding to the effective tendencies (5.4.7c), (5.4.7d), and with the homogeneous boundary conditions (5.4.3). Forces in round brackets in (5.4.7c) -(5.4.7d) compensate each other, mainly, and the resulting effective tendency $\hat{\mathbf{F}}_\mathbf{v}$ remains restricted in the BRZ. The major compensation is achieved due to the application of nonhomogeneous boundary conditions (5.4.6). These conditions supply the solution ϕ_c with a long-wave component, which compensates the initial large $\mathbf{F_v}$, restoring the approximate geostrophic balance and providing the initial tendency to be moderate.

In this respect, substitution of $\mathbf{F_v}$ to $\mathbf{F_v} - \hat{\mathbf{G}}\phi_\mathbf{c}$ gives an effect, similar to the background surface pressure field initialization from the coarser model. Consequently, the conditions (5.4.6) are rather essential, and the proper specification of the normal component of hydrostatic tendency $\mathbf{F_v}$ on the boundary Γ is of great significance. Fortunately, the thermic and Coriolis forcings, both being reliably computable from the temperature and wind distributions, are major contributors to this tendency.

The temperature and ω tendencies are not affected by the described modification (5.4.5) - (5.4.7d), and remain (5.4.2c), and (5.3.3), respectively.

Though the described scheme with $\hat{p}_0$ in the role of lower model surface is more rigorous in comparison with the former one, its advantage is, that it provides some lowering of numerical noise, if $\hat{p}_0$ is chosen appropriately smooth. Along with the application of $\hat{p}_0$, and when the background temperature $T_0(p)$ is introduced into consideration, it is advantageous to apply one more noise-lowering modification, which consists in the prior separation of the background thermic geopotential in (3.4.4b)

$$\varphi(x, y, p, t) = \varphi_0(p) + \varphi'(x, y, p, t) \ . \qquad (5.4.8a)$$

The mean component depends on the background temperature only

$$\varphi_0(p) = gh(x, y) + R_d \int_p^{\overline{p}_0(x,y)} \frac{T_0(p')}{p'} dp' \ , \qquad (5.4.8b)$$

where R_d is the gas constant of the dry air, whereas the fluctuative part is a function of the fluctuative part of RT

$$\varphi'(x, y, p, t) = \int_p^{\overline{p}_0(x,y)} \frac{(RT)'(x, y, p', t)}{p'} dp'$$

$$= \int_p^{\overline{p}_0(x,y)} \frac{(RT)(x, y, p', t) - R_d T_0(p')}{p'} dp' \ . \qquad (5.4.8c)$$

Cancellation of φ_0 dependence on x, y occurs due to the barometric formula (2.5.7c). Due to this cancellation, the hydrostatic tendency will not include the large background geopotential φ_0, which will enhance smoothness of the numerically computed $\mathbf{F_v}$.

When applied in the discrete scheme, the tendencies (5.2.4), (5.2.5) are modified to

$$F_{ui+1/2jk} = -\left[\frac{1}{\overline{\overline{h_x}^x}}\left(-\overline{Z\overline{\overline{h_x}^y V}^x}^y + \delta_x E + \frac{\overline{\overline{h_x m\dot{\eta}}^x \Delta_\eta u}^\eta}{\overline{\Delta_\eta p}^x}\right)\right]_{i+1/2jk}$$

$$-(\widetilde{G}_x\overline{\varphi'}^\eta)_{i+1/2jk} + (P_u + K_u)_{i+1/2jk} \ , \qquad (5.4.9a)$$

$$F_{vij+1/2k} = -\left[\frac{1}{\overline{\overline{h_y}^y}}\left(\overline{Z\overline{\overline{h_y}^x U}^y}^x + \delta_y E + \frac{\overline{\overline{h_y m\dot{\eta}}^y \Delta_\eta v}^\eta}{\overline{\Delta_\eta p}^y}\right)\right]_{ij+1/2k}$$

$$-(\widetilde{G}_y\overline{\varphi'}^\eta)_{ij+1/2k} + (P_v + K_v)_{ij+1/2k} \ , \qquad (5.4.9b)$$

where φ' is computed from the recurrence (which is a modification of (5.1.17))

$$\varphi'_{ijNlev+1/2} = 0 \ ,$$

$$\overline{\varphi'}^\eta_{ijk} = \varphi'_{ijk+1/2} + \frac{1}{2}(RT)'_{ijk}\alpha_{ijk} \ , \qquad (5.4.10)$$

$$\varphi'_{ijk-1/2} = \overline{\varphi'}^\eta_{ijk} + \frac{1}{2}(RT)'_{ijk}\alpha_{ijk} \ .$$

Note that there is no linearization in connection with the separation (5.4.8a), and the equation for the full temperature remains (5.4.2c).

6 Explicit Eulerian time scheme

6.1 Time scheme

Integration of equations (5.4.2a) – (5.4.2c) (or (5.4.7a), (5.4.7b), (5.4.2c), respectively, when the separation (5.4.5) is applied) is implemented as the explicit-Eulerian leapfrog time-stepping scheme, which is a parallel option to the ordinary, hydrostatic explicit-Eulerian integration scheme. Nonhydrostatic integration is switched on with the logical key *nhdyn*. The integration block–scheme in the nonhydrostatic regime is presented in Fig. 6.1.1.

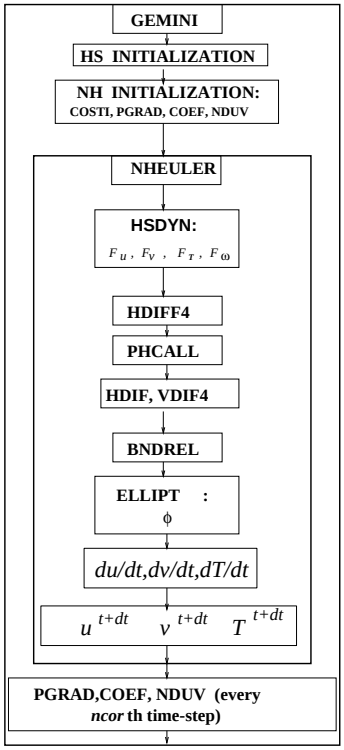

Fig. 6.1.1

In the main routine GEMINI, subroutines COSTI, PGRAD, COEF, and NDUV are called after general initialization. The subroutine COSTI initializes coefficients for fast 2D cosine-Fourier transformation. The subroutine PGRAD computes $\overline{p}_0$, which in the present realization is the initial actual hydrostatic surface pressure, and prepares difference arrays $\Delta_\eta p$, $\Delta_x p$. The subroutine COEF prepares coefficients for the elliptic solver, including the mean temperature $< T >_k$, mean pressure $< p >_{k+1/2}$, and vertical eigenvectors and eigenvalues of the mean elliptic operator. The routine NDUV checks the balance (5.1.9) of the vertically integrated mass and restores the balance if there exists any initial departure.

The restoration algorithm is as follows. The imbalance

$$d = \left(\frac{\partial \overline{p}_0}{\partial t} + \sum_{k=1}^{Nlev} (\nabla \cdot \mathbf{V})_k \right)^{(in)} \tag{6.1.1}$$

is computed and then a gradiental correction is introduced into the velocity field:

$$\mathbf{v}_k^{(fin)} = \mathbf{v}_k^{(in)} - \nabla\zeta \ , \tag{6.1.2}$$

where ζ is the solution of the equation

$$\nabla \cdot (\overline{p}_0 \nabla\zeta) = d. \tag{6.1.3}$$

This equation is inverted iteratively with fast cosine-Fourier transformation. The corrected velocity field (6.1.2) satisfies the balance condition (5.1.9).

The recalculation of boundary pressure field $\overline{p}_0$ in PGRAD, coefficients in COEF and restoration of the mass balance with NDUV is applied repeatedly after each *ncor* time-step.

In the main Eulerian time-stepping routine NHEULER, which represents a modification of the hydrostatic subroutine EULER, the subroutine HSDYN (represents a modification of DYN) is called, which computes the hydrostatic tendencies $F_u,\ F_v,\ F_T$, and F_ω in accordance with (5.2.4), (5.2.5), (5.2.9), and (5.3.3b). Thereafter, the explicit horizontal spectral smoothing (optional) for $u,\ v,\ ,T$, and humidity q is carried out in HDIFF4 which is followed by physical parametrization in PHCALL. The explicit smoothing and physical parametrization are common with the hydrostatic model. After that there is another branching: instead of the implicit smoothing with DIFFH, in the nonhydrostatic case a spectral smoothing is performed by subroutines HDIF and VDIF4. The subroutine HDIF represents an implicit diffusive spectral filter of variable order. It makes use of the cosine-Fourier transformation and acts on the Fourier amplitude $\tilde{\psi}_{ijk}$ of the field ψ (in the role of ψ are $u,\ v$, and T') as follows

$$(\tilde{\psi}_{ijk})^{(fin)} = \frac{\tilde{\psi}_{ijk}^{(in)}}{1 + \gamma_k^h[(\lambda_i^x + \lambda_j^y)/(\lambda_{Nlon/2}^x + \lambda_{Nlat/2}^y)]^{q_k}} \ . \tag{6.1.4a}$$

Here γ_k^h and q_k are the level-dependent smoothing parameters, and $\lambda^x,\ \lambda^y$ represent the eigenvalues of one-dimensional horizontal Laplacians (see (5.3.12), and Appendix C, (C.1c)). The default value for γ_k^h is 1, though in the short-scale domain ($dx, dy < 10$ km) γ_k must be increased to avoid buoyancy wave reflection at the top. The parameter q varies with the height according to

$$q_k = 2 - \exp[-(k-1)^2/k_h^2] \ , \tag{6.1.4b}$$

the default value for k_h is 5. Thus, in the majority of the atmosphere, $q_k = 2$ and the filter has fourth order, whereas at the top, where $q_k \to 1$, it steadily transforms to a second order filter.

The explicit vertical 4th order filter VDIF4 performs smoothing (Miranda and James 1992)

$$\psi_{ijk}^{fin} = (1 - \gamma_k^v)\psi_{ijk}^{in} - \gamma_k^v \left(\psi_{ijk+2} + \psi_{ijk-2} - 4\psi_{ijk+1} - 4\psi_{ijk-1}\right)^{in} \quad . \quad (6.1.5a)$$

The parameter γ_k^v is a piecewise linear function of the level index

$$\gamma_k^v = \begin{cases} \gamma_{min}^v & \text{if } k > k_v, \\ \gamma_{min}^v + (\gamma_{max}^v - \gamma_{min}^v)\frac{k_v - k}{k_v - 1} & \text{if } k \le k_v. \end{cases} \quad (6.1.5b)$$

The default values of the parameters are $k_v = Nlev$, $\gamma_{min}^v = 0.0$, $\gamma_{kax}^v = 0.0625$. Note that $\gamma^v = 0.0625$ yields total elimination of the 2-grid-length waves.

TABLE 6.1.1

The nonhydrostatic tuning parameters in the namelist NAMRUN and common COMNHD

Name	Type	Default	Reference
lnhdyn	logical	.false.	NH switch
lncor	logical	.false.	Switch for COEF and NDUV
ncor	integer	50	Period in time-steps for COEF and NDUV
lhdif	logical	.false.	Switch for (6.1.4)
rkh	real	5.0	k_h in (6.1.4b)
lvdif4	logical	.false.	Switch for (6.1.5)
nkv	integer	Nlev	k_v in (6.1.5b)
gvmin	real	0.0	γ_{min}^v in (6.1.5b)
gvmax	real	0.0625	γ_{max}^v in (6.1.5b)
epsell	real	5.e-4	ε in (5.3.4e)

Smoothing is followed by the boundary relaxation in BNDREL, which is an ordinary boundary relaxation subroutine of the hydrostatic HIRLAM.

Thereafter, the hydrostatic tendencies are passed to the subroutine ELLIPT, in which the baric geopotential is computed. Finally, NHEULER is finished by the tendency updating with nonhydrostatic contributions and by the next time level prognostic field computation. The tuning parameters of the nonhydrostatic model are presented in Table 6.1. In the program they are described in the common COMNHD.INC with default initialization in the routine NAMEIN, and they can be initialized explicitly in the namelist NAMRUN.

6.2 Numerical tests

The developed NH model is tested in two different regimes: (A) nonhydrostatic forecast on low-resolution ("hydrostatic") grids with realistic initial data and with the physics included. These simulations should be considered as preliminary experiments, which will be extensively continued after code parallelization. (B) nonhydrostatic simulations on high-resolution grids in the adiabatic regime without the physics, with artificial initial and boundary data and model orography.

Modeling is performed in the single-processor environment on Pentium II. The time step Δt is in all experiments chosen maximal for that particular resolution. It is determined by the Courant-Friedrichs-Lewy stability condition

$$\Delta t < \Delta x/(U + C) \ , \tag{6.2.1}$$

where Δx is the horizontal grid-step, U is the dominant horizontal wind-speed, and C is the typical phase speed of buoyancy waves. As the external waves are excluded, C represents the internal buoyancy wave phase speed. It is $\sim 100 - 150$ m/s at large scales but diminishes rapidly as the horizontal scale decreases. The typical time-step is 90 s at the 22 km resolution, 60 s at the 11 km resolution, 50 s at the 2.2 km resolution (for $U = 25$m/s), and 30 s at the 1 km resolution (for $U = 25$ m/s). Presumably, at the high-resolution limit ($\Delta x, \Delta y \leq 5$ km), where $C << U$, the explicit scheme reaches theoretical upper limit $\Delta x/U$.

A. Low–resolution tests with physics

Experiments in the realistic conditions are carried through at the 22 and 11 km resolutions. Integration is performed with the non-hydrostatic extension

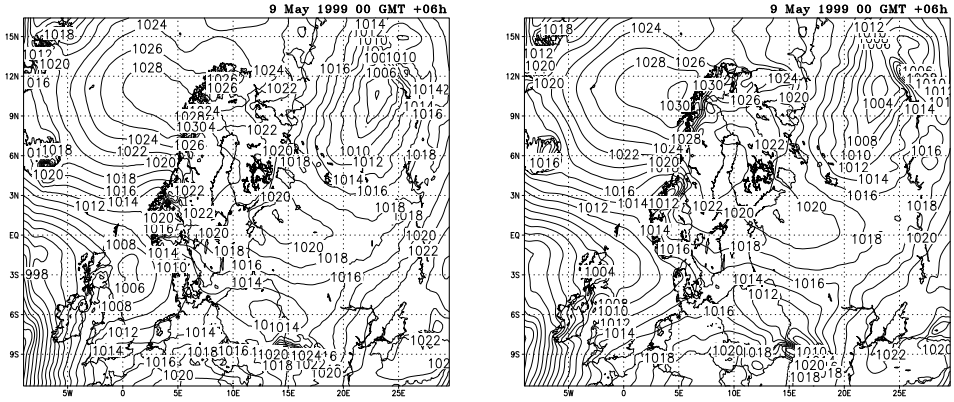

(a) hydrostatic model (b) nonhydrostatic model

Fig.6.2.1 6h forecast of surface pressure with the explicit hydrostatic (a) and nonhydrostatic model (b). 194×140 grid, 31 levels, 22 km resolution.

of HIRLAM 4.6.0, and thus, the physical package represents the physics of version 4.6.0.

The purpose of 22-km-resolution experiments is to check the influence of the surface pressure adjustment and to demonstrate, that this does not reduce model quality in the hydrostatic domain. Another purpose is to show that the plane approximation in the main part of elliptic operator does not influence model performance in the case of moderate (square side less than 5000 km) integration area. Integration is performed with the 31 level, 194x140 points (4300 km × 3100 km) model. The time step is 90 s, and the default spectral smoothing is applied. The results of 6h forecasts of the sea-level pressure are shown in Fig. 6.2.1, where the nonhydrostatic model is compared with the explicit (20 s time-step), hydrostatic Eulerian scheme. As seen from the example, results by NH model are close to the corresponding results of the hydrostatic scheme, though not identical. The comparison shows also, that there is no systematic distortion of nonhydrostatic pressure forecast to the edges of the area due to the quasi-plane approximation of the elliptic equation.

The results of 24 hour forecast with the 11 km resolution on the 114×100 points grid (1210 km×1100 km) for the sea-level pressure are shown in Fig.

6.2.2, and for the vertical cross-section of u-wind and temperature, in Fig. 6.2.3. The time step in these experiments is 60 s. The forecasts by the NH model and semi-implicit Eulerian hydrostatic model are compared with the analysis for the same time. The sea-level surface pressure distributions (Fig. 6.2.2) of hydrostatic and nonhydrostatic models show reasonable coincidence. Spectral smoothing in the NH model is reduced in comparison with the default standard to the values: $\gamma_k^h = 0.5$, $\gamma_{min}^v = 0$, and $\gamma_{max}^v = 0.01$. In spite of that, the NH scheme produces smoother wind distribution in the middle troposphere than the hydrostatic model (Fig. 6.2.3). At the same time, the nonhydrostatic scheme exhibits wind anomaly at the top, which is caused by

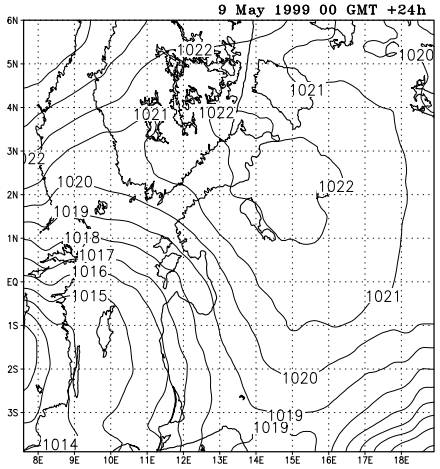

(a) hydrostatic model

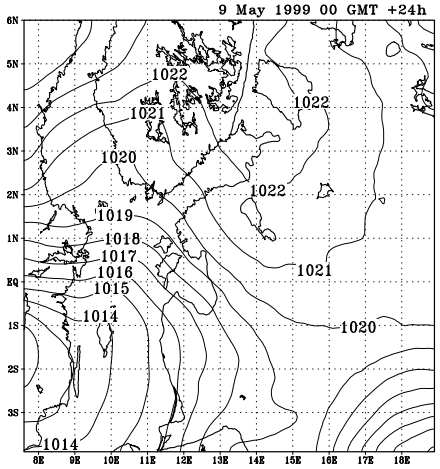

(b) nonhydrostatic model

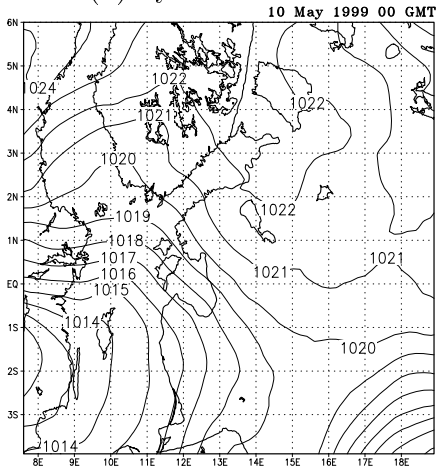

(c) analysis

Fig. 6.2.2. 24 h forecast of surface pressure with the hydrostatic model (a), and nonhydrostatic model (b); (c) - analysis for the same time. Grid size 114×100 points, 31 levels, 11 km resolution.

residual buoyancy-wave reflection on the upper boundary and which shows that the level of spectral smoothing is too low in the top region. However, the close co-incidence of the two models during a rather continuous run shows that the NH kernel does work and produces reliable results.

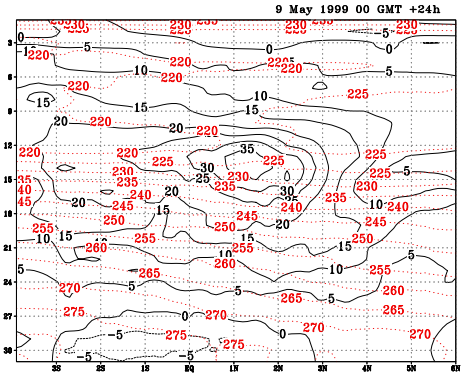

(a) hydrostatic model

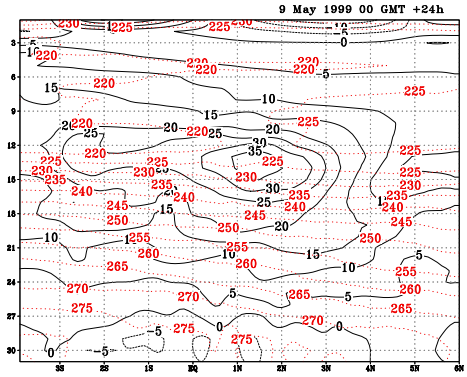

(b) nonhydrostatic model

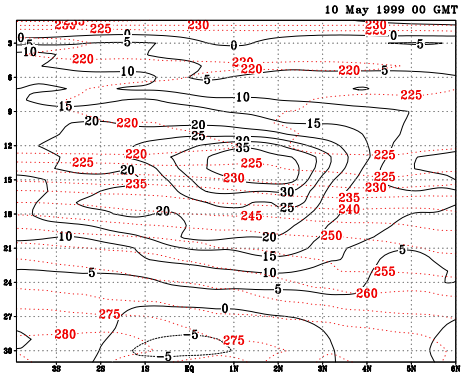

(c) analysis

Fig. 6.2.3. The 24 h vertical cross sections (along the meridian 14E on the local grid) of temperature and u-component of wind. (a) - hydrostatic model, (b) - nonhydrostatic model, (c) - analysis. Grid size 114×100 points, 31 levels, 11 km resolution.

B. High–resolution adiabatic tests

High-resolution experimentation in the adiabatic mode has been the main tool for model debugging and nonhydrostatic kernel quality testing. Following examples aim at demonstrating the quality of the model in actually nonhydrostatic conditions and clearing up its high-resolution limit. These are experiments with artificial orography and initial state of the atmosphere.

NH HIRLAM, N=0.0185 1/s

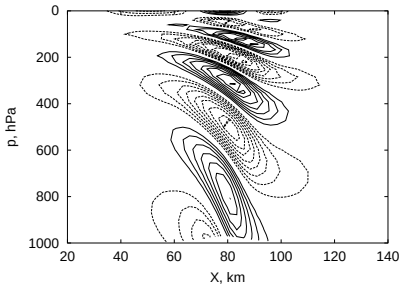

Analytical model, N=0.0185 1/s

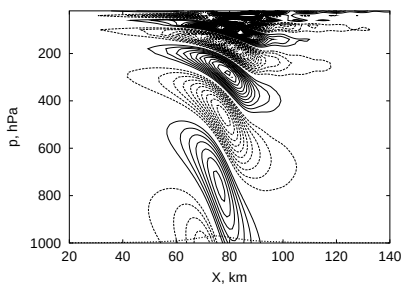

NH HIRLAM, N=0.01 1/s

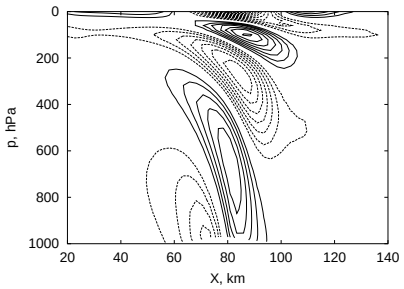

Analytical model, N=0.01 1/s

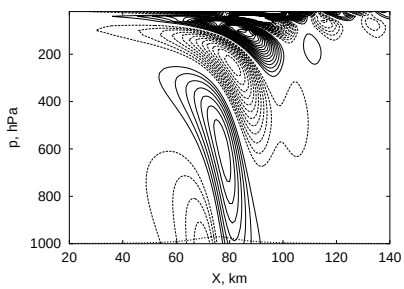

Fig. 6.2.4 Vertical velocity waves in the case of the stationary flow over one-dimensional isolated mountain. a = 10 km, h_0 = 300 m, U = 25 m/s. *Isoline step* Δw *= 0.1 m/s. Grid 65×49, resolution 2.2 km,* Δt *= 40 s; Nstep = 240;* u, v *:* γ_k^h *= 2.5; T:* γ_k^h *= 7.5, nbdpts = 6.*

Orography is presented by an isolated bell-shape mountain

$$h(x,y) = \frac{h_0}{[1 + (x/a_x)^2 + (y/a_y)^2]^s} \ , \tag{6.2.1}$$

where a_x, a_y represent half-widths of the hill along x and y axes, and nondimensional parameter $s \sim 1$ (usually 1 or 1.5). The special case of one-dimensional orography is modeled with the formula

$$h(x,y) = \frac{h_0}{1 + (x/a)^2} \ . \tag{6.2.1$'$}$$

The initial state is characterized with the sea-level temperature T = 280 K, Väisälä frequency $N(p)$, and wind U, which is taken initially constant and then transformed to the mass-balanced wind with the help of formulae (6.1.1) - (6.1.3). The corresponding mean surface pressure field $\overline{p}_0$ is computed from the barometric formula. Consequently, the algorithm with the background baric geopotential separation (5.4.5) is employed along with

(a) Temperature T, ΔT =0.1 K

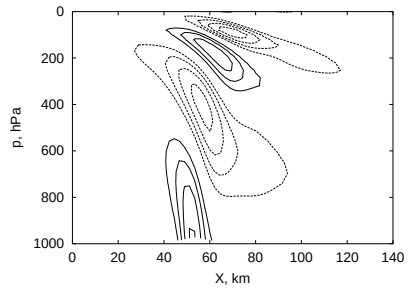

(b) Wind u, Δu =0.25 m/s

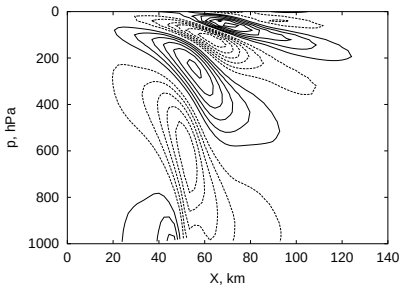

(c) Wind w, Δw =0.1 m/s

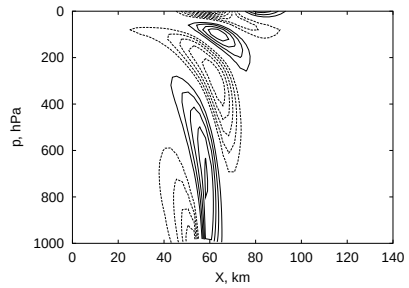

(d) Wind w, Δw = 0.1 m/s

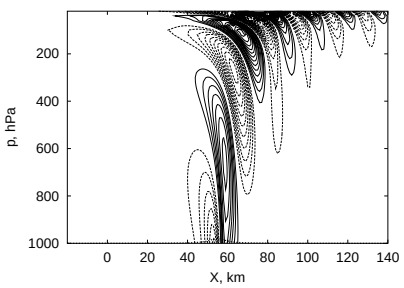

Fig. 6.2.5 Nonhydrostatic steady flow over one-dimensional isolated mountain, according to HIRLAM (panels a - c) and the analytical model (panel d). a = 5 km, h_0 = 200 m, U = 25 m/s, N = 0.01 1/s. *Grid 100×50, resolution 2.2 km,* Δt *= 50 s, Nstep = 216,* γ_k^h *= 4 for* u*,* v*, and* γ_k^h *= 8 for* T*, nbdpts = 8.*

the temperature and thermic geopotential splittings (3.5.1), and (5.4.8). The boundary-relaxed time integration scheme is (5.4.2c) (5.4.7a), and (5.4.7b) in this case. Boundary conditions are presented by the boundary fields, which coincide with the background fields: $u_b = U$, $v_b = 0$, $T_b = T_0(p)$.

The difference between the one and two dimensional orography in boundary handling consists in the BRZ treatment. In the case of two-dimensional hill (6.2.1), the boundary fields are specified on all boundary walls, whereas in the case of one-dimensional orography (6.2.1'), boundary relaxation is applied on the west wall $i = 1$ and east wall $i = Nlon$. In the case of one-dimensional orography, there is no relaxation at the south and north boundaries, which is equivalent to a continuation of the domain of integration to $\pm\infty$ in the

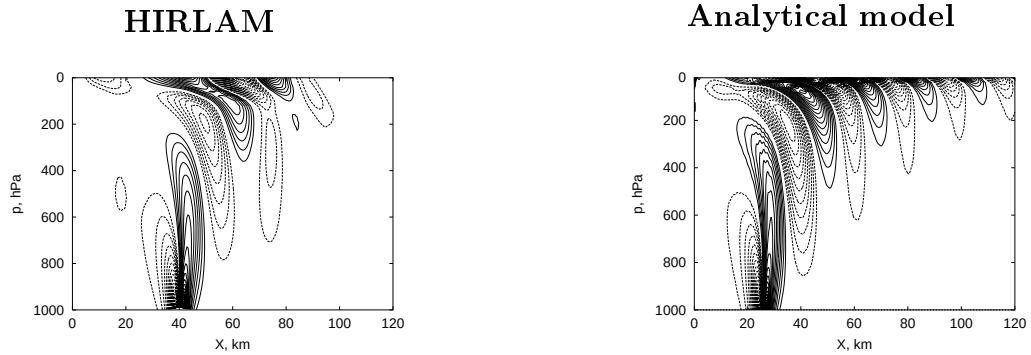

Fig. 6.2.6 Vertical velocity waves in the case of the stationary flow over one-dimensional isolated mountain. a = 2 km, h_0 = 100 m, U = 15 m/s, N = 0.005 1/s, isoline step Δw = 0.02 m/s. *Grid 257×49, resolution 0.4 km, Δt = 20 s, Nstep = 500, γ_k^h = 25 for u, v, and γ_k^h = 50 for T, nbdpts = 20.*

y–direction. Evolution of the atmosphere is modeled from the initial state until the stationary flow regime is reached with required precision. The final wind, temperature, and surface pressure fields are compared with the semi-analytical solutions of the linearized equations where available.

A series of stationary two-dimensional flows over one-dimensional orography (6.2.1') in different conditions is presented in Figures 6.2.4 - 6.2.7. The main nonhydrostatic flow characteristic, nondimensional parameter aN/U, varies from 7.4 in Fig. 6.2.4, which corresponds to the hydrostatic flow regime, to 0.66 in Figs. 6.2.5 and 6.2.6, which represents completely nonhydrostatic flows. The main attribute of the nonhydrostatic behavior is the leeward shift of the wave sequence with height. At the relatively long nonhydrostatic scales a = 10 and 5 km (Figs. 6.2.4, 6.2.5), the shift is small and becomes evident at the higher levels only, whereas at the shorter scale a = 2 km, all waves are leeward shifted. The resolution (grid-step) is 2.2 km (Figs. 6.2.4 and 6.2.5), 1 km (Fig. 6.2.6), and 0.4 km (Figs. 6.2.6 and 6.2.7). Along with the decrease of the horizontal scale (determined by the mountain half-width) and stability parameter N, the horizontal smoothing parameter γ_k^k in (6.1.4a) should be increased to avoid numerical noise and reflection at the top. Theoretically, there is no reflection for constant N in the continuous model. However, due to the finite vertical resolution and fluctuations of N, the reflection does exist in the numerical model, and a sponge layer, modeled

by spectral filters (6.1.4) and (6.1.5), is necessary at the top. Parameter γ_k^h can be varied in a broad interval. Its enlargement causes the increase of smoothing rate and reduction of the wave amplitude, whereas reduction causes larger noise and spurious wave reflection near the top, and forces a time step decrease. Vertical diffusive smoothing (6.1.5) is the default one in all experiments, as the model is relatively insensitive to the small variation of γ_k^v, while the large variation is not supported by the explicit filter.

Experimentation with one-dimensional orography is a sensitive indicator of model quality. Vertical oscillations of the atmosphere are strongest in this case, as the atmosphere can not flow around the obstacle, yet is forced to get over it. Both wave amplitudes and vertical extent of wave pattern are reduced in the case of two-dimensional obstacle. An experiment with two-dimensional orography (6.2.1), $a_x = a_y = 1$ km, $h_0 = 200$ m, $s = 1.5$ is shown in Fig. 6.2.8. As seen, vertical flow disturbances are restricted below the 800 hPa level (though modeling is performed for the complete vertical extent of the atmosphere).

The general conclusion from the presented experiments is that the model is capable of nonhydrostatic simulation. In comparison with the linear model there is some reduction of wave amplitude and narrowing of wave wings due to spectral diffusion (especially manifested near the top of the atmosphere) but both the general wave pattern and the nonhydrostatic lee-ward shift are reproduced authentically.

As experimentation shows, the grid-point extent *nbdpts* of the BRZ must be increased along with the resolution. In Fig. (6.2.4), and (6.2.5) with $\Delta x, \Delta y = 2.2$ km, $bndpts = 6$ and 8, respectively. In the high-resolution (0.4 km) experiment with two-dimensional hill in Fig. 6.2.8, this parameter is $nbdpts = 8$ (which is yet not too extreme), while in the experiments with one–dimensional mountains with the same resolution (Figs. 6.2.6 and 6.2.7), $bndpts = 20$ and 16, respectively. The reason for the large grid-point extent of the BRZ is the potential buoyancy wave reflection in narrower BRZs. The reflection would be much stronger in the case of one-dimensional orography, as wave amplitudes are larger in this case and they do not decrease significantly during propagation from the mountain to the boundary. This explains larger *nbdpts* in one-dimensional experiments. However, the situation would be similar for a small-scale two-dimensional hill, placed near the outer boundary. For practical reason of rapidly increasing computational cost, the reasonable value of *nbdpts* is restricted within $nbpts = 10$, and even

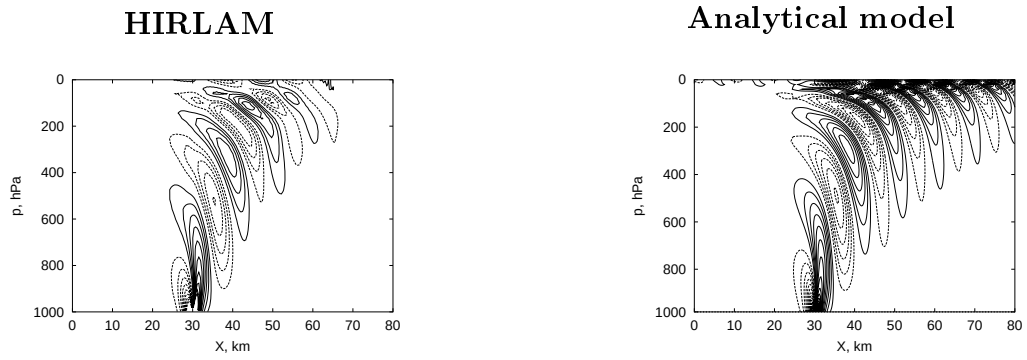

Fig. 6.2.7 Vertical velocity waves in the case of the stationary flow over one-dimensional isolated mountain. a = 1 km, h_0 = 200 m, U = 15 m/s, N = 0.01 1/s, isoline step Δw = 0.05 m/s. *Grid 257×49, resolution 0.4 km; Δt = 20 s; Nstep = 300; γ_k^h = 35, nbdpts = 16.*

in extreme situations it should not go beyond 15 - 20. This limitation sets, for a nonhydrostatic model with the BRZ, the practical upper limit of horizontal resolution at 0.5 - 1 km.

7 Conclusions

In this part the theoretical concept of the nonhydrostatic, pressure-coordinate, anelastic model of atmospheric dynamics has been brought to the numerical code. Preliminary experimentation with the new code has shown its ability to produce reliable results both in hydrostatic and nonhydrostatic regions. It is premature, of course, to make far-reaching conclusions before thorough and careful testing of the new routine. However, the model has shown its potential in these preliminary runs, and some conclusions can be already made.

The present maximum horizontal resolution of the model is approximately 0.5 km. This limit is set by gravity wave reflection at the lateral boundaries. To achieve the 0.5 km resolution without meaningful reflection, the boundary relaxations zone depth must be 15 - 20 points. For higher resolutions, either this depth should be increased even more (which is non-realistic), or lateral boundaries should be made transparent to buoyancy waves.

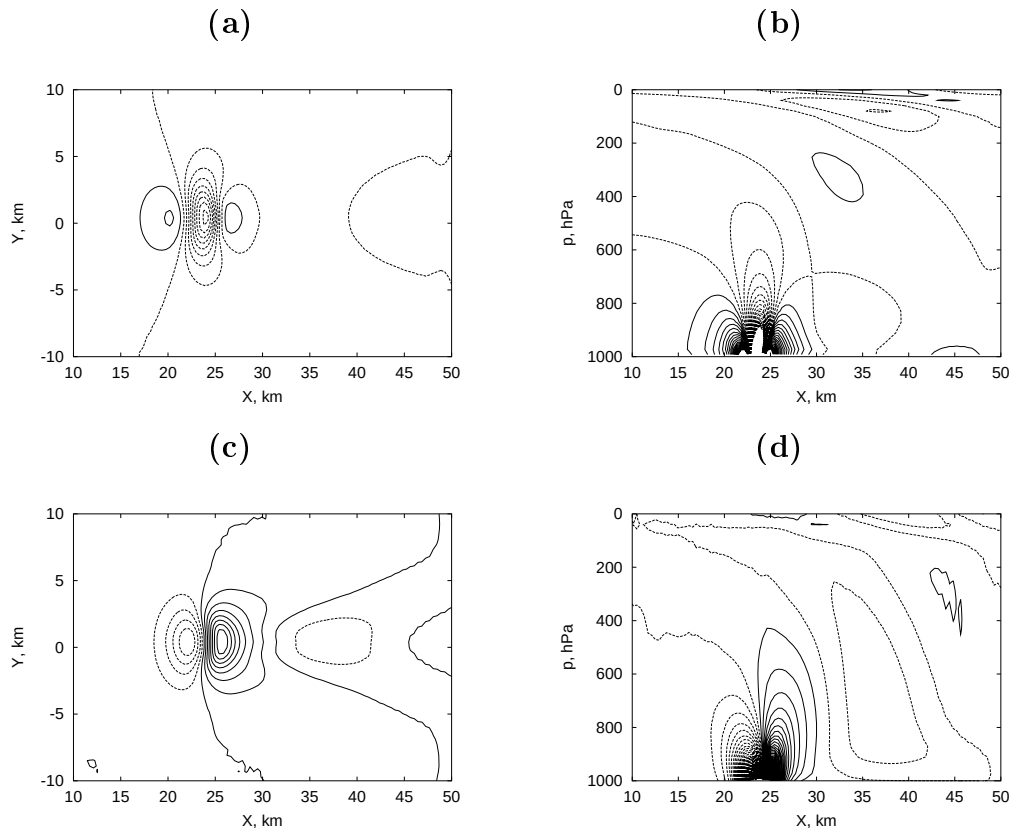

Fig. 6.2.8 Distributions of u and w components of wind at the stationary flow over the circular hill. $a_x = a_y = 1$ km, $h_0 = 200$ m, U = 15 m/s, N = 0.005 1/s. *Grid 129×97, resolution 0.4 km, $\Delta t = 20$ s, Nstep = 300; u, v, T : $\gamma_k^h = 20$, nbdpts = 8.* Isoline interval 0.01 m/s.
(a) – u at the level $p = 860$ hPa, (b) – u at the vertical plane $y = 0$, (c) – w at the level $p = 860$ hPa, (d) – w at the vertical plane $y = 0$.

The model is economical in terms of vertical resolution requirements. The standard 31-level eta-grid provides sufficient resolution for adiabatic dynamics at all horizontal scales. However, much higher vertical resolution may be needed by diabatic processes. So far, tests with the finer vertical grid are missing.

Due to the application of surface pressure adjustment, the accessible time step is rather large and makes the model applicable in high-resolution simulations already in its present explicit–mode realization. In the high-resolution domain ($\Delta x < 5$ km), the time step reaches the theoretical upper limit and most likely can not be significantly increased with the help of a semi–implicit scheme. At larger scales, where the main limiting factor is the internal buoyancy wave speed, the implicit scheme would approximately double the present time-step.

The practical advantage of the model is that it supports instant inclusion of existing physics. Still, at finer scales, beginning with 11 km resolution, physical parametrization should be revised.

Acknowledgements

This investigation has the financial support of the Estonian Science Foundation under Grant 2624.

A. Männik has the grant for PhD studies offered by the Väisälä Foundation at the Finnish Academy of Sciences.

8 References

Haltiner, G.J., Williams, R.T., 1980:*Numerical Prediction and Dynamic Meteorology.* John Wiley and Sons, 477 p.

Källén, E. (Editior), 1996: *HIRLAM Documentation Manual.*

Miller, M. J., Pearce, R. P., 1974: A three-dimensional primitive equation model of cumulonimbus convection. *Q. J. R. Meteorol. Soc.*, **100,** 133–154

Miranda, P. M. A. and James, I. N. 1992 Non-linear three-dimensional effects on gravity-wave drag: splitting flow and breaking waves. *Q. J. R. Meteorol. Soc.*, **118,** 1057–1081

Press, H.W., Teukolsky, S.A., Vettering, W.T., Flannery, B.P., 1992: *Numerical Recipes in FORTRAN*, Cambridge University Press, 961 p.

Rõõm, R., 1997: *Nonhydrostatic Atmospheric Dynamics in Pressure-Related Co-*

ordinates. Grant of the Estonian Science Foundation No. 172, Final Report. Tartu Observatory, 102 pp.

Rõõm R., Männik A., 1999: On the development of a nonhydrostatic version of HIRLAM. In: *HIRLAM 4 Workshop Report, Workshop on High Resolution Modeling, Norrköping, 10-12 May 1999*, 89 - 99.

Xue, M., Thorpe, A. J., 1991: A mesoscale numerical model using the nonhydrostatic pressure-based sigma-coordinate equations: Model experiments with dry mountain flows. *Mon. Wea. Rev.*, **119,** 1168–1165.

White, A.A. ,1989: An extended version of nonhydrostatic, pressure coordinate model. *Q. J. R. Meteorol. Soc.*, **115**, 1243 – 1251.

Williams, G. P. 1969 Numerical integration of the three-dimensional Navier-Stokes equations for incompressible flow. *J. Fluid Mech.*, **37**, 727–750.

Appendix A

Pressure gradient $\hat{\mathbf{G}}$ and divergence $\hat{\mathbf{G}}^+$ in the discrete model

Integration of divergence (5.1.12) gives

$$\int dVm\hat{\mathbf{G}}^+ \cdot \mathbf{v} \approx \sum_{ijk} \Delta x \Delta y (\Delta_\eta p h_x a h_y \hat{\mathbf{G}}^+ \cdot \mathbf{v})_{ijk}$$

$$= \Delta x \Delta y \sum_{ijk} \left[\delta_x \left(\overline{h_y}^x \overline{\Delta_\eta p}^x u \right) - \Delta_\eta \left(h_y \overline{\overline{u}^\eta \delta_x p}^x \right) \right.$$

$$\left. + \delta_y \left(\overline{h_x}^y \overline{\Delta_\eta p}^y v \right) - \Delta_\eta \left(h_x \overline{\overline{v}^\eta \delta_y p}^y \right) \right]_{ijk} . \qquad (A.1)$$

Due to the full differences in the square brackets, this integral transforms to a surface integral (disappears for finite u and v). Thus, (5.1.12) defines the divergence, indeed.

To get the alternative form (5.1.12'), the identity

$$[\delta_\xi (\overline{s}^\xi v)]_i = (s \delta_\xi v)_i + (\overline{v \delta_\xi s}^\xi)_i \qquad (A.2)$$

is required. With the help of this identity, the first term in the first square bracket of (5.1.12) can be modified

$$\delta_x \left(\overline{h_y}^x \overline{\Delta_\eta p}^x u \right) = \Delta_\eta p \delta_x (\overline{h_y}^x u) + \overline{\overline{h_y}^x u \delta_x \Delta_\eta p}^x ,$$

whereas the second term (with η in the role of ξ) can be presented

$$\Delta_\eta \left(\overline{\overline{h_y}^x \overline{u}^\eta \delta_x p}^x \right) = \overline{\overline{h_y}^x u \delta_x \Delta_\eta p}^x + \overline{\overline{h_y}^x (\Delta_\eta u) \delta_x p}^{x\eta} \ .$$

Analogical identities hold for the second square bracket. As a result, (5.1.12') follows.

To derive the operator $\hat{\mathbf{G}}$ skew conjugate to $\hat{\mathbf{G}}^+$, the integral relationship (4.1.16) has to be used, which for the λ-component is

$$\sum_{ijk} (h_x h_y \Delta_\eta p \varphi \hat{G}_x^+ u)_{ijk} = - \sum_{ijk} (\overline{h_x}^x \overline{h_y}^x \overline{\Delta_\eta p}^x u \hat{G}_x \varphi)_{i+1/2jk} \ . \qquad (A.3)$$

Using definition (5.1.12), left side here is

$$\sum_{ijk} (h_x h_y \Delta_\eta p \varphi \hat{G}_x^+ u)_{ijk} = \sum_{ijk} \varphi_{ijk} \left[\delta_x \left(\overline{h_y}^x \overline{\Delta_\eta p}^x u \right) - \Delta_\eta \left(\overline{\overline{h_y}^x \overline{u}^\eta \delta_x p}^x \right) \right]_{ijk} \qquad (A.4)$$

To the first term in the sum an identity is applied

$$\sum_i a_i (\delta_x b)_i = - \sum_i b_{i+1/2} (\delta_x a)_{i+1/2} \ ,$$

where finite functions are assumed. Further, this identity is denoted shortly as

$$a_i (\delta_x b)_i \sim - b_{i+1/2} (\delta_x a)_{i+1/2} \ . \qquad (A.5)$$

Thus "$\sim$" means "equivalent at the summation over finite functions". Analogical identity is applied to the second term in (A.4)

$$a_k (\Delta_\eta b)_k \sim - b_{k+1/2} (\Delta_\eta a)_{k+1/2} \ , \qquad (A.6)$$

along with

$$(\overline{a}^\eta)_{k+1/2} (b)_{k+1/2} \sim (a)_k (\overline{b}^\eta)_k \ . \qquad (A.7)$$

This results in the formula

$$\sum_{ijk} (h_x h_y \Delta_\eta p \varphi \hat{G}_x^+ u)_{ijk} =$$

$$- \sum_{ijk} (\overline{h_x}^x \overline{h_y}^x \overline{\Delta_\eta p}^x)_{i+1/2jk} u_{i+1/2jk} \left[\frac{1}{\overline{\overline{h_x}^x}} \delta_x \varphi - \frac{1}{\overline{h_x}^x \overline{\Delta_\eta p}^x} \overline{(\delta_x p) \Delta_\eta \overline{\varphi}^x}^\eta \right]_{i+1/2jk} \ ,$$

from which presentation (5.1.13) follows for $\hat{G}_x$ and $\hat{G}_y$.

In further applications, the following equivalences (which proceed from the definitions of $\hat{\mathbf{G}}$ and $\hat{\mathbf{G}}^+$) are also useful:

$$(h_x h_y \Delta_\eta p \varphi \hat{G}_x^+ u)_{ijk} \sim -(\overline{h_x}^x \overline{h_y}^x \overline{\Delta_\eta p}^x u \hat{G}_x \varphi)_{i+1/2jk} \ , \qquad (A.8a)$$

$$(h_x h_y \Delta_\eta p \varphi \hat{G}_y^+ v)_{ijk} \sim -(\overline{h_x}^y \overline{h_y}^y \overline{\Delta_\eta p}^y v \hat{G}_y \varphi)_{ij+1/2k} \ . \qquad (A.8b)$$

The first one represents (A.3), the second is its y-coordinate analogue.

In a small domain, when $|\tan\theta| < 1$, divergence (5.1.12) can be simplified, considering the metrical coefficients $h_x = \cos\theta$ and $h_y = 1$ constants

$$(\hat{\mathbf{G}}^+ \cdot \mathbf{v})_{ijk} = \left[\frac{1}{h_x}\delta_x(u) - \frac{\overline{(\Delta_\eta u)\delta_x p}^{x\eta}}{h_x \Delta_\eta p} + \frac{1}{h_y}\delta_y(v) - \frac{\overline{(\Delta_\eta v)\delta_y p}^{y\eta}}{h_y \Delta_\eta p} \right]_{ijk} \ , \qquad (A.8)$$

which means a plane approximation for $\hat{\mathbf{G}}^+$. This approximation was applied in initial versions of the nonhydrostatic model (Rõõm and Männik 1999). Yet it does not yield much simplification in comparison with more precise representation (5.1.12') and is not applied in the recent versions.

Appendix B

Energetics in the discrete model

Total energy of the discrete model is

$$E = \frac{\Delta x \Delta y}{g} \sum_{ijk} E_{ijk} \ , \qquad (B.1)$$

where E_{ijk} is the energy, associated with the cell with indexes $\{i, j, k\}$:

$$E_{ijk} = E_{\mathbf{v}ijk} + E_{wijk} + E_{Tijk} \ ,$$

$$E_{\mathbf{v}ijk} = \frac{1}{2}\left[\left(\overline{h_x}^x \overline{h_y}^x \overline{\Delta_\eta p}^x u^2 \right)_{i+1/2jk} + \left(\overline{h_x}^y \overline{h_y}^y \overline{\Delta_\eta p}^y v^2 \right)_{ij+1/2k} \right]$$

$$E_{wijk} = \frac{1}{2}\left[h_x h_y \overline{\Delta_\eta p}^\eta \frac{(w^s)^2}{2} \right]_{ijk+1/2} \ ,$$

$$E_{Tijk} = [h_x h_y (\Delta_\eta p) c_p T]_{ijk} \ .$$

Applying to E_{ijk} differentiation in time yields with the use of equations (5.2.1), (5.2.2), (5.2.3), and (5.3.3) (dissipative P- and K-terms are omitted)

$$\frac{\partial E_{ijk}}{\partial t} = b^z_{ijk} - b^E_{ijk} - b^T_{ijk} - b^w_{ijk} + b^\varphi_{ijk} + b^\phi_{ijk} \qquad (B.2)$$

where

$$b^z_{ijk} = \left(\overline{h_y}^x U \overline{Z\overline{h_x}^y V}^x\right)_{i+1/2jk} - \left(\overline{h_x}^y V \overline{Z\overline{h_y}^x U}^y\right)_{ij+1/2k} \qquad (B.3a)$$

$$b^E_{ijk} = \left[\overline{h_y}^x \left(U\delta_x E + u\overline{\overline{h_x m\dot{\eta}}^x \Delta_\eta u}^\eta\right)\right]_{i+1/2jk} + \left[\overline{h_x}^y \left(V\delta_y E + v\overline{\overline{h_y m\dot{\eta}}^y \Delta_\eta v}^\eta\right)\right]_{ij+1/2k} \qquad (B.3b)$$

$$b^T_{ijk} = (h_x h_y \Delta_\eta p c_p \hat{a} T)_{ijk} = \left\{c_p[\overline{h_y U\delta_x T}^x + \overline{h_x V\delta_y T}^y + h_x h_y \overline{(m\dot{\eta})\Delta_\eta T}^\eta]\right\}_{ijk} \qquad (B.3c)$$

$$b^w_{ijk} = [h_x h_y \overline{\Delta_\eta p}^\eta w^s(\hat{a}w^s)]_{ijk+1/2} = [\overline{h_y\overline{U}^\eta \delta_x w^s}^x + \overline{h_x\overline{V}^\eta \delta_y w^s}^y + h_x h_y \overline{\overline{m\dot{\eta}}^\eta \Delta_\eta w^s}^\eta]_{ijk+1/2} \qquad (B.3d)$$

$$b^\varphi_{ijk} = -\left(\overline{h_x}^x \overline{h_y}^x U\widetilde{G}_x\overline{\varphi}^\eta\right)_{i+1/2jk} - \left(\overline{h_x}^y \overline{h_y}^y V\widetilde{G}_y\overline{\varphi}^\eta\right)_{ij+1/2k} + (h_x h_y \Delta_\eta p)_{ijk}\left(\frac{RT\omega}{p}\right)_{ijk} \qquad (B.3e)$$

$$b^\phi_{ijk} = -\left(\overline{h_x}^x \overline{h_y}^x U\hat{G}_x\phi\right)_{i+1/2jk} - \left(\overline{h_x}^y \overline{h_y}^y V\hat{G}_y\phi\right)_{ij+1/2k} + \left(h_x h_y \frac{wp}{\overline{\overline{H}^\eta}}\Delta_\eta\phi\right)_{ijk+1/2} \qquad (B.3f)$$

For energy conservation, the right hand terms in (B.2) should at the summation either transform to surface integrals as full differences or mutually annihilate in neighboring nodes.

In (B.3a), an equivalence holds (equivalence "$\sim$" is defined in Appendix A) for the first term

$$\left(\overline{h_y}^x U \overline{Z\overline{h_x}^y V}^x\right)_{i+1/2jk} \sim \left(\overline{\overline{h_y}^x U}^y Z\overline{\overline{h_x}^y V}^x\right)_{i+1/2j+1/2k}$$

and analogous equivalence holds for the second term. As a result, (B.3a) transforms to a surface integral.

In (B.3b), equivalences are valid

$$\left(\overline{h_y}^x u\overline{\overline{h_x m\dot{\eta}}^x \Delta_\eta u}^\eta\right)_{i+1/2jk} \sim \left(\overline{h_y}^x \overline{h_x m\dot{\eta}}^x \overline{u}^\eta \Delta_\eta u\right)_{i+1/2jk+1/2} =$$

$$\left(\overline{h_y}^x\overline{h_x m\dot\eta}^x\Delta_\eta\frac{u^2}{2}\right)_{i+1/2jk+1/2}\sim\left[h_xh_ym\dot\eta\Delta_\eta\left(\frac{1}{h_y}\overline{h_y}^x\overline{\frac{u^2}{2}}^x\right)\right]_{ijk+1/2}.$$

Analogically,

$$\left(\overline{h_x}^y v\overline{\overline{h_ym\dot\eta}^y\Delta_\eta v}^\eta\right)_{ij+1/2k}\sim\left[h_xh_ym\dot\eta\Delta_\eta\left(\frac{1}{h_x}\overline{h_x}^y\overline{\frac{v^2}{2}}^y\right)\right]_{ijk+1/2}.$$

Thus,

$$b^E_{ijk}\sim\left(\overline{h_y}^xU\delta_xE\right)_{i+1/2jk}+\left(\overline{h_x}^yV\delta_yE\right)_{ij+1/2k}+\left(h_xh_ym\dot\eta\Delta_\eta E\right)_{ijk+1/2}\sim$$

$$\left(\overline{\overline{h_y}^xU\delta_xE}^x+\overline{\overline{h_x}^yV\delta_yE}^y+\overline{h_xh_ym\dot\eta\Delta_\eta E}\eta\right)_{ijk}.$$

Addition to this relationship of the identity $0=(E\ D)_{ijk}$, where

$$D_{ijk}\equiv\left[\delta_x\left(\overline{h_y}^xU\right)+\delta_y\left(\overline{h_x}^yV\right)+\Delta_\eta\left(h_xh_ym\dot\eta\right)\right]_{ijk}=0\qquad(B.4)$$

is equal to zero due to (5.1.8), results in

$$b^E_{ijk}\sim\left[\delta_x\left(\overline{h_y}^x\overline{E}^xU\right)+\delta_y\left(\overline{h_x}^y\overline{E}^yV\right)+\Delta_\eta\left(h_xh_y\overline{E}^\eta m\dot\eta\right)\right]_{ijk}.$$

The discrete divergence of a vector on the right side will give at the summation a surface integral.

Analogical addition of identity $0=c_pTD$ to (B.3c) yields

$$b^T_{ijk}=\left[\delta_x\left(\overline{h_y}^x\overline{c_pT}^xU\right)+\delta_y\left(\overline{h_x}^y\overline{c_pT}^yV\right)+\Delta_\eta\left(h_xh_y\overline{c_pT}^\eta m\dot\eta\right)\right]_{ijk}.$$

Quite similar is also transformation of (B.3d) to a divergent form. First, with the help of (A.7)

$$b^w_{ijk}\sim$$

$$(\overline{U}^\eta\overline{h_x}^y\overline{w^s}^x\delta_xw^s)_{i+1/2jk+1/2}+(\overline{V}^\eta\overline{h_y}^x\overline{w^s}^y\delta_yw^s)_{ij+1/2k+1/2}+(h_xh_y\overline{m\dot\eta}^\eta\overline{w^s}^\eta\Delta_\eta w^s)_{ijk}$$

$$=\left(\overline{U}^\eta\overline{h_x}^y\delta_x\frac{(w^s)^2}{2}\right)_{i+1/2jk+1/2}+\left(\overline{V}^\eta\overline{h_y}^x\delta_y\frac{(w^s)^2}{2}\right)_{ij+1/2k+1/2}+\left(h_xh_y\overline{m\dot\eta}^\eta\Delta_\eta\frac{(w^s)^2}{2}\right)_{ijk}$$

$$\sim\left(U\overline{h_x}^y\delta_x\overline{\frac{(w^s)^2}{2}}^\eta\right)_{i+1/2jk}+\left(V\overline{h_y}^x\delta_y\overline{\frac{(w^s)^2}{2}}^\eta\right)_{ij+1/2k}+\left(h_xh_ym\dot\eta\Delta_\eta\overline{\frac{(w^s)^2}{2}}^\eta\right)_{ijk+1/2}.$$

A full divergence results from this relationship after addition of identity $0 = D\overline{(w^s)^2}^{\eta}/2$.

The relation (B.3e) can be used for specification of discrete representation of the energy conversion term $RT\omega/p$. First, (B3.e) is presented in the form

$$b^{\varphi}_{ijk} = b^1_{ijk} + b^2_{ijk} \ ,$$

where

$$b^1_{ijk} = -\left(\overline{h_x}^x \overline{h_y}^x U \hat{G}_x \overline{\varphi}^{\eta}\right)_{i+1/2jk} - \left(\overline{h_x}^y \overline{h_y}^y V \hat{G}_y \overline{\varphi}^{\eta}\right)_{ij+1/2k} + (h_x h_y \Delta_{\eta} p)_{ijk} \left(\frac{RT\omega}{p}\right)_{ijk}$$

corresponds to the exact gradient $\hat{\mathbf{G}}$, and

$$b^2_{ijk} = -\left(\overline{h_x}^x \overline{h_y}^x U(\widetilde{G}_x - \hat{G}_x)\overline{\varphi}^{\eta}\right)_{i+1/2jk} - \left(\overline{h_y}^x \overline{h_y}^y V(\widetilde{G}_y - \hat{G}_y)\overline{\varphi}^{\eta}\right)_{ij+1/2k} =$$

$$-\left[\overline{h_y}^x u\left(\overline{\delta_x p \overline{\Delta_{\eta}\varphi}^{\eta x}}^{\eta} - \overline{\delta_x p}^{\eta}\overline{\Delta_{\eta}\varphi}^x\right)\right]_{i+1/2jk} - \left[\overline{h_x}^y v\left(\overline{\delta_y p \overline{\Delta_{\eta}\varphi}^{\eta y}}^{\eta} - \overline{\delta_y p}^{\eta}\overline{\Delta_{\eta}\varphi}^y\right)\right]_{ij+1/2k}$$

represents a modification due to approximation $\hat{\mathbf{G}} \ \rightarrow \ \widetilde{G}$.

Application of the equivalences (A.8) to b^1_{ijk} results in

$$b^1_{ijk} \sim \left[h_x h_y (\Delta_{\eta} p)\left(\overline{\varphi}\hat{\mathbf{G}}^{+} \cdot \mathbf{v} + \frac{RT\omega}{p}\right)\right]_{ijk} \ ,$$

which can be presented with the help of (5.1.14) as

$$b^1_{ijk} \sim \left[h_x h_y \left(-\overline{\varphi}^{\eta}\Delta_{\eta}\omega + (\Delta_{\eta} p)\frac{RT\omega}{p}\right)\right]_{ijk} \ .$$

Using equivalences (A.7) and (A.5), the first term can be transformed further:

$$-\left(h_x h_y \overline{\varphi}^{\eta}\Delta_{\eta}\omega\right)_{ijk} \sim -\left(h_x h_y \varphi \Delta_{\eta}\overline{\omega}^{\eta}\right)_{ijk+1/2} \sim \left(h_x h_y \overline{\omega}^{\eta}\Delta_{\eta}\varphi\right)_{ijk} \ .$$

Thus,

$$b^1_{ijk} \sim \left[h_x h_y \left(\overline{\omega}^{\eta}\Delta_{\eta}\varphi + (\Delta_{\eta} p)\frac{RT\omega}{p}\right)\right]_{ijk} \ .$$

The term b^2_{ijk} can be transformed, applying to the first terms in the round brackets equivalence (A.7) twice in respect of η:

$$b^2_{ijk} \sim -\left[\overline{h_y}^x \left(\overline{u^{\eta}\delta_x p}^{\eta} - u\overline{\delta_x p}^{\eta}\right)\overline{\Delta_{\eta}\varphi}^x\right]_{i+1/2jk} - \left[\overline{h_x}^y \left(\overline{v^{\eta}\delta_y p}^{\eta} - v\overline{\delta_y p}^{\eta}\right)\overline{\Delta_{\eta}\varphi}^y\right]_{ij+1/2k}$$

$$= -\left[\frac{\overline{h_y}^x}{4}\Delta_\eta\left(\delta_x p\Delta_\eta u\right)\overline{\Delta_\eta\varphi}^x\right]_{i+1/2jk} - \left[\frac{\overline{h_x}^y}{4}\Delta_\eta\left(\delta_y p\Delta_\eta v\right)\overline{\Delta_\eta\varphi}^y\right]_{ij+1/2k}$$

$$\sim -\frac{1}{4}\left[\left(\overline{\overline{h_y}^x\Delta_\eta\left(\delta_x p\Delta_\eta u\right)}^x + \overline{\overline{h_x}^y\Delta_\eta\left(\delta_y p\Delta_\eta v\right)}^y\right)\Delta_\eta\varphi\right]_{ijk} .$$

Thus,

$$b^\varphi_{ijk} \sim \left[h_x h_y\left(\overline{\omega}^\eta\Delta_\eta\varphi + (\Delta_\eta p)\frac{RT\omega}{p}\right)\right]_{ijk} -$$

$$\frac{1}{4}\left[\left(\overline{\overline{h_y}^x\Delta_\eta\left(\delta_x p\Delta_\eta u\right)}^x + \overline{\overline{h_x}^y\Delta_\eta\left(\delta_y p\Delta_\eta v\right)}^y\right)\Delta_\eta\varphi\right]_{ijk} .$$

This expression cannot be simplified further, and for energy conservation the right side should vanish to give

$$\left(\frac{RT\omega}{p}\right)_{ijk} = -\left(\Omega\frac{\Delta_\eta\varphi}{\Delta_\eta p}\right)_{ijk} \qquad (B.5a)$$

where

$$\Omega_{ijk} = \overline{\omega}^\eta_{ijk} - \left[\frac{\overline{\overline{h_y}^x\Delta_\eta\left(\delta_x p\Delta_\eta u\right)}^x + \overline{\overline{h_x}^y\Delta_\eta\left(\delta_y p\Delta_\eta v\right)}^y}{4h_y h_x}\right]_{ijk} . \qquad (B.5b)$$

Finally, with the help of (A.8) and (5.2.12), an equivalence follows for (B.3f):

$$b^\phi_{ijk} \sim (h_x h_y)_{ij}\left\{[\phi(\Delta_\eta p)\hat{\mathbf{G}}^+\cdot\mathbf{v}]_{ijk} - (\omega\Delta_\eta\phi)_{ijk+1/2}\right\} ,$$

which can be further transformed with the help of (A.7) to

$$b^\phi_{ijk} \sim (h_x h_y\phi\Delta_\eta p)_{ijk}\left(\hat{\mathbf{G}}^+\cdot\mathbf{v} + \frac{\Delta_\eta\omega}{\Delta_\eta p}\right)_{ijk} .$$

Due to (5.1.14), expression in the large round brackets is zero.

Thus, we have shown that energy is conserved in the employed discretization scheme. A single non-trivial additional relationship, required for energy conservation, is the expression (B.5) for the energy-conversion term.

Appendix C
Orthogonal bases

Horizontal bases X and Y

For X and Y the discrete normalized cosine bases are employed,

$$X_{iq} = \begin{cases} \frac{1}{\sqrt{2(Nlon-1)}} \ , q = 1 \\ 2\frac{\cos[\pi(i-1)(q-1)/(Nlon-1)]}{\sqrt{2(Nlon-1)}} \ , q = 2, ...Nlon-1 \\ \frac{(-1)^{i-1}}{\sqrt{2(Nlon-1)}} \ , q = Nlon \end{cases} \qquad (C.1a)$$

$$Y_{jr} = \begin{cases} \frac{1}{\sqrt{2(Nlat-1)}} \ , r = 1 \\ 2\frac{\cos[\pi(j-1)(r-1)/(Nlat-1)]}{\sqrt{2(Nlat-1)}} \ , r = 2, ...Nlat-1 \\ \frac{(-1)^{j-1}}{\sqrt{2(Nlat-1)}} \ .r = Nlat \end{cases} \qquad (C.1b)$$

They are solutions of the eigen-problems (see (5.3.12))

$$(\mathcal{L}_x X_q) = -\lambda_q^x X_q \ , \quad (\mathcal{L}_y Y_r) = -\lambda_r^y Y_r \ ,$$

where and λ_q^x, λ_r^y are

$$\lambda_q^x = \frac{4}{\langle h_x \rangle^2 \Delta x^2} \sin^2\left(\frac{\pi}{2}\frac{q-1}{Nlon-1}\right) \quad \lambda_r^y = \frac{4}{\langle h_y \rangle^2 \Delta y^2} \sin^2\left(\frac{\pi}{2}\frac{r-1}{Nlat-1}\right) \ . \ (C.1c)$$

Two successive cosine transformations perform the identity transformation: $XX = I$, $YY = I$, which means that the inverse transformations coincide with the direct transformations

$$X^{-1} = X \ , \qquad Y^{-1} = Y \ . \qquad (C.2)$$

Vertical basis.

The eigenvalue-problem for vertical Laplacian (see (5.3.12)) is

$$\sum_{k'} (\mathcal{L}_\eta)_{kk'} E_{k's} = -\lambda_s^\eta E_{ks} \ , \qquad (C.3)$$

with $\mathcal{L}_\eta$, presented by (5.3.9c). With the help of transformation

$$E_{ks} = e_{ks}/\sqrt{\langle \Delta p \rangle_s}, \qquad (C.4)$$

The equation (C.3) can be presented in the symmetrical form

$$\sum_{k'=k-1}^{k+1} M_{k,k'} e_{k's} = -\lambda_s^\eta e_{ks} \ , \quad k, \ s \ = \ 1, ..., Nlev \ , \tag{C.5}$$

where M is a symmetrical tridiagonal matrix

$$M_{kk} = -\frac{\beta_{k-1/2} + \beta_{k+1/2}}{\langle \Delta p \rangle_k} \ , \quad M_{k,k+1} = M_{k+1,k} = \frac{\beta_{k+1/2}}{(\langle \Delta p \rangle_k \langle \Delta p \rangle_{k+1})^{1/2}} \ , \tag{C.6a}$$

$$\beta_{k+1/2} = \frac{\langle p \rangle^2_{k+1/2}}{\langle \overline{H}^\eta \rangle^2_{k+1/2} \overline{\langle \Delta p \rangle}^\eta_{k+1/2}} \ , \tag{C.6b}$$

$$\text{for } k \ = \ 1, ..., Nlon - 1,$$

and

$$M_{Nlev,Nlev} = -M_{Nlev-1,Nlev} \ . \tag{C.6c}$$

This is a negative semi-definite matrix: it has one (with index $s = 1$ by agreement) null–eigenvalue

$$\lambda_1^\eta = 0$$

with the corresponding eigenvector

$$e_{ks} = c\sqrt{\langle \Delta p \rangle_s},$$

where c is constant, whereas other eigenvalues are real and positive $\lambda_s^\eta \ > \ 0$, $s \ = \ 2, ..., Nlon$.

Inverse to e is the matrix

$$e^{-1}_{kl} = e_{lk}$$

and thus, inverse of E in accordance with (C.4) is

$$E^{-1}_{ks} = \sqrt{\langle \Delta p \rangle_k} e_{ks} \ . \tag{C.7}$$

Except the first one, eigenvectors and eigenvalues must be solved from (C.3) numerically. There exist multiple recipes and ready free-ware for computation of eigenvectors and eigenvalues of symmetric, tri-diagonal, negative/semi-negative matrixes. In the NH HIRLAM the routine *tqli* from *Recipes* (Press *et al*, 1992) is applied.

Appendix D
Iterative algorithm for lateral boundary forces f

The derivation of iterative equations (5.3.15), (5.3.16) is similar for all four groups of coefficients $\tilde{f}^{xl(l)}$, $\tilde{f}^{xr(l)}$, $\tilde{f}^{yl(l)}$, $\tilde{f}^{yr(l)}$, and we will follow in detail the derivation of $\tilde{f}^{xl(l)}$ from the first condition in (5.3.11e). Applying to this relationship the Fourier transformation in x and η coordinates, $Y^{-1}E^{-1}$, and using (5.3.13) for presentation of ϕ, we get

$$\frac{1}{\langle h_x\rangle\Delta x}\sum_q (X_{2q}-X_{1q})\tilde{\phi}^{(l)}_{qrs} = \tilde{a}^{xl}_{rs}\ . \qquad (D.1)$$

Let us present $\tilde{\phi}$ in (5.3.14) with explicitly exposed $f^{xl(l)}$:

$$\tilde{\phi}^{(l)}_{qrs} = -\frac{c^x\tilde{f}^{xl(l)}X_{q,1}}{\lambda^x_q+\lambda^y_r+\lambda^\eta_s} + \tilde{\phi}^{xl(l)}_{qrs}\ , \qquad (D.2)$$

where the last term represents the remaining part of (5.3.14), including all other boundary coefficients $f^{xr(l)}$, $f^{yl(l)}$, $f^{yr(l)}$, and $\tilde{\gamma}^{(l)}$. Substitution of (D.2) into (D.1) and making use of $c^x = 2/(\langle h_x\rangle\Delta x)$ results in

$$\tilde{f}^{xl(l)} = \frac{1}{s^x_{rs}}\left(\tilde{a}^{xl}_{rs} - \sum_q \frac{X_{2q}-X_{1q}}{\langle h_x\rangle\Delta x}\tilde{\phi}^{xl(l)}_{qrs}\right)\ , \qquad (D.3)$$

where

$$s^x_{rs} = -\frac{2}{(\langle h_x\rangle\Delta x)^2}\sum_q \frac{(X_{2q}-X_{1q})X_{q,1}}{\lambda^x_q+\lambda^y_r+\lambda^\eta_s}\ .$$

The explicit presentation of s^x_{rs} with the help of (C.1a) yields (5.3.17a).

The equation (D.3) includes unknown coefficients f and γ also on the right side, and thus, for the specification of boundary coefficients, similar equations are needed for f on other lateral walls, and for γ, and the arising system should be considered and solved *in corpore*. However, the second, summation term on the right hand of (D.3) is small for smooth $\phi^{xl(l)}$, which assumes smoothness of the volume-distributed source A^v and boundary gradients a. In Fourier terms, smoothness of ϕ means that the coefficients $\tilde{\phi}^{xl(l)}$ are essentially different from zero for small indexes q only([1]). For very small q, r, s which assume a very narrow spectrum $\tilde{a}$ of normal

[1]It is worth of pointing out, that for small q, the first term in the right hand sum approximates the derivative of the continuous cosine at the zero, which is the continuous sine at the zero, which is zero.

gradients (i.e., extreme smoothness of a), and for $Nlon, Nlat \to \infty$, which means continuous limit of the model, one has

$$s^x_{rs}, \;\; \to \;\; 1 \; , \qquad \frac{X_{2q} - X_{1q}}{\langle h_x \rangle \Delta x} \;\; \to \;\; 0 \; ,$$

and, as a consequence,

$$\tilde{f}^{xl(l)} \to \tilde{a}^{xl}_{rs} \; , \tag{$D.4$}$$

which yields the first relationship in (5.3.7).

For smooth $\mathcal{A}^v$ and a, but for finite $Nlon, Nlat, Nlev$, the second term in (D.3) is still small, and it can be approximated in the iterative scheme from the previous iteration $(l-1)$:

$$\tilde{f}^{xl(l)} = \frac{1}{s^x_{rs}} \left(\tilde{a}^{xl}_{rs} - \sum_q \frac{X_{2q} - X_{1q}}{\langle h_x \rangle \Delta x} \tilde{\phi}^{xl(l-1)}_{qrs} \right) \; . \tag{$D.5$}$$

Presenting in (D.4)

$$\tilde{f}^{xl(l)} = \tilde{f}^{xl(l-1)} + \delta \tilde{f}^{xl(l)} \; , \tag{$D.6$}$$

we obtain

$$\delta \tilde{f}^{xl(l)} = \frac{1}{s^x_{rs}} \left(\tilde{a}^{xl}_{rs} - \sum_q \frac{X_{2q} - X_{1q}}{\langle h_x \rangle \Delta x} \tilde{\phi}^{(l-1)}_{qrs} \right) \; . \tag{$D.7$}$$

(Note the full coefficient of the previous iteration $\tilde{\phi}^{(l-1)}$ on the right side). This equation is the equation (5.3.16a), written in a different way.

The first iterative solution of (D.6) - (D.7) is

$$\tilde{f^{xl}_{rs}}^{(1)} = \tilde{a}^{xl}_{rs} / s^x_{rs} \; , \tag{$D.8$}$$

which already takes into account the finite resolution of the model. As $0 < s^x_{rs}, s^y_{qs} < 1$ for finite $Nlon, Nlat$, the spectral coefficients (D.8) are larger than predicted by the smooth approximation (D.4).